Measurement report: Intensive biomass burning emissions and rapid nitrate formation drive severe haze formation in Sichuan basin, China: insights from aerosol mass spectrometry

Zhier Bao[1], Xinyi Zhang[1], Qing Li[1], Jiawei Zhou[1], Guangming Shi[2], Li Zhou[2], Fumo Yang[2], Shaodong Xie[3], Dan Zhang[4], Chongzhi Zhai[4], Zhenliang Li[4], Chao Peng[4], and Yang Chen[1]

[1] Chongqing Institute of Green and Intelligent Technology, Chinese Academy of Sciences, Chongqing, 400714, China

[2] Department of Environmental Science and Engineering, College of Architecture and Environment, Sichuan University, Chengdu 610065, China

[3] SKL-ESPC and BIC-ESAT, College of Environmental Sciences and Engineering, Peking University, Beijing 100871, China

[4] Academy of Environmental Science, Chongqing, 401147, China

Correspondence: Yang Chen (chenyang@cigit.ac.cn)

Abstract

Haze pollution is a severe environmental problem, caused by elevation of fine particles (aerodynamic diameter < 2.5 μm, $PM_{2.5}$), which is related to secondary aerosol formation, unfavourable synoptic conditions, regional transport, etc. The regional haze formation in basin areas, along with intensive emission of precursors, high relative humidity and poor dispersion conditions, is still limitedly understood.In this study, a field campaign was conducted to investigate the factors resulting in haze formation in Sichuan Basin (SCB) during winter in 2021. The fine aerosol chemical composition was characterised by using a time-of-flight aerosol chemical speciation monitor (ToF-ACSM), which also provided detailed information on the sources for organic aerosols (OA). The average concentration of non-refractory fine particles (NR-$PM_{2.5}$) was 98.5 ± 38.7 μg/m^3, and organics aerosols, nitrate, sulphate, ammonium, and chloride took up 40.3, 28.8, 10.6, 15.3 and 5.1 % of $PM_{2.5}$. Three factors, including a hydrocarbon-like OA (HOA), a biomass burning OA (BBOA), and an oxygenated OA (OOA), were identified by applying the positive matrix factorisation (PMF)

28 analysis, and they constituted 24.2, 24.2 and 51.6 % of OA on average, respectively. Nitrate

29 formation was promoted by gas-phase and aqueous-phase oxidation, while sulphate was mainly

30 formed through aqueous-phase process. OOA showed strong dependence on Ox, demonstrating the

31 contribution of photooxidation to OOA formation. OOA concentration increased as aerosol liquid

32 water content (ALWC) increased within 200 $\mu g/m^3$ and kept relatively constant when ALWC > 200

33 $\mu g/m^3$, suggesting the insignificant effect of aqueous-phase reactions on OOA formation. Among

34 the three haze episodes identified during the whole campaign, the driving factors were different: the

35 first haze episode (H1) was driven by nitrate formation through photochemical and aqueous-phase

36 reactions, and the second haze episode (H2) was mainly driven by the intense emission of primary

37 organic aerosols from biomass burning and vehicle exhaust, while the third haze episode (H3) was

38 mainly driven by reactions involving nitrate formation and biomass burning emission. HOA and

39 BBOA were scavenged, while OOA, nitrate, and sulphate formation were enhanced by aqueous-

40 phase reactions during fog periods, which resulted in the increase of O:C from pre-fog to post-fog

41 periods. This study revealed the factors driving severe haze formation in SCB, and implied the

42 benefit of controlling nitrate as well as intense biomass burning and vehicle exhaust emission to the

43 mitigation of heavy aerosol pollution in this region.

1. Introduction

Although a series of emission reduction strategies had been implemented to mitigate severe haze pollution over a decade in China, the fine particle (particulate matter with aerodynamic diameter less than 2.5 μm, $PM_{2.5}$) pollution events still occurred, especially during autumn and winter (Ding et al., 2019; Zhao et al., 2020; Yan et al., 2020). Haze formation was affected by the intense emission of primary particles, rapid formation of secondary aerosols, stagnant meteorological conditions, and topography. The interplay among these factors usually makes haze formation complex (Bao et al., 2019; Guo et al., 2014; Zheng et al., 2015), which resulted in difficulties in making air pollution mitigation strategies.

Many studies showed that the rapid increase of secondary aerosols (including secondary inorganic/organic aerosols, i.e., SIA and SOA) played an important role in haze formation (Huang et al., 2014; Wu et al., 2022). Nitrate, sulphate, and ammonium, mainly formed through photochemical oxidation and aqueous-phase reactions in the atmosphere, were the major component of SIA. Previous studies demonstrated that the substantial formation of nitrate and sulphate exacerbated severe haze development (Wang et al., 2020; Liu et al., 2020). For example, Zheng et al. (2016) investigated the factors driving haze formation in Beijing in 2013, and the results showed that the enhanced production of sulphate and nitrate led to their increased contribution to $PM_{2.5}$ as the pollution level increased, while the contribution of organic matter (OM) decreased. The emission of SO_2 had been reduced dramatically over the past ten years in China; however, NOx did not show a significant reduction (Zhou et al., 2021; Liu et al., 2019). Thus, the haze formation was found to be mainly driven by the reactions generating nitrate in recent year (Fu et al., 2020; Li et al., 2018; Zhai et al., 2021).

Compared to SIA, the formation process of SOA was more complicated (Chen et al., 2017). For instance, SOA could be formed through the gas-phase photooxidation of volatile organic compounds (VOCs), which was affected by temperature, relative humidity (RH), and total organic aerosol mass loadings (Clark et al., 2016; Hinks et al., 2018; Donahue et al., 2006). SOA could also be formed through the oxidation of water-soluble VOCs or organic products of gas-phase photochemistry, which was observed in the field and laboratory studies (Liu et al., 2018; Chen et al., 2015). Besides, the aging of primary organic aerosols (POA) by oxidants in the atmosphere also

76   contributed to SOA (Wang et al., 2021; Gilardoni et al., 2016). For instance, the organic aerosols

77   emitted from biomass burning were oxidised through the photochemical oxidation process driven

78   by OH radicals which might take place in both gas and aqueous phases (Paglione et al., 2020). The

79   variations of regional and seasonal emissions might also affect the formation of SOA (Dai et al.,

80   2019; Sun et al., 2016). Thus, it is of vital importance to consider various factors when investigating

81   SOA formation.

82   Similar to the city clusters such as Beijing, Shanghai and Guangzhou in North China Plain

83   (NCP), Yangtze River Delta (YRD) and Pearl River Delta (PRD), the Chengdu-Chongqing city

84   cluster, located in the Sichuan Basin (SCB) in Southwest China, is also suffering severe haze

85   pollution (Tao et al., 2017; Tan et al., 2019). Many efforts had been made to investigate the temporal

86   variation, chemical composition and formation mechanism of $PM_{2.5}$ during the evolution of haze

87   episodes in NCP, YRD and PRD (Peng et al., 2021; Sun et al., 2016; Zhang et al., 2015; Yan et al.,

88   2020), whereas, only a few studies focused on the factors resulting in haze formation in SCB (Zhang

89   et al., 2019; Song et al., 2019). These studies mainly focused on the formation of inorganic species

90   in $PM_{2.5}$, and the results showed that the rapid formation of SIA under high RH conditions promoted

91   the increase of $PM_{2.5}$. However, further studies on the characteristics of OA, including the temporal

92   evolution, sources and formation pathways, are still lacking.

93   The area of SCB is ~260,000 $km^{2,}$ and its population is ~110 million, making it an important

94   developing region in Southwest China. The basin is a subtropical expanse of low hills and plains

95   and is completely encircled by high mountains and plateaus, which is unfavourable for either

96   horizontal transport or vertical diffusion. The atmosphere in SCB was characterised by persistently

97   high relative humidity and low wind speed all year round. The haze evolution in SCB might be

98   different from those in other regions due to its unique topography, meteorological conditions and

99   emission sources, which remained unclear. Therefore, comprehensive studies are needed to reveal

100   the key factors contributing to haze formation in the basin (Wang et al., 2018).

101   The Time-of-Flight Aerosol Chemical Speciation Monitor (ToF-ACSM) is a robust and highly

102   sensitive instrument that provides real-time characterisation and composition of non-refractory

103    $PM_1/PM_{2.5}$ (NR-PM_1/$PM_{2.5}$) depending on the type of the aerodynamic lens used (Liu et al., 2007;

104   Xu et al., 2017). Compared to the Aerodyne aerosol spectrometer (AMS), the ToF-ACSM is more

105   compact and cheaper. However, the ToF-ACSM does not figure particle sizing. Compared to the

106 quadrupole-ACSM (Q-ACSM), the ToF-ACSM has better mass resolution and detection limits

107 (Fröhlich et al., 2013). Although the ToF-ACSM had not been widely deployed in field observations

108 as AMS/Q-ACSM did in a number of different sites over China, it had successfully characterised

109 the variation of $PM_1/PM_{2.5}$ and the sources of organic aerosols in the cities within NCP, YRD and

110 PRD (Ge et al., 2022; Sun et al., 2020; Guo et al., 2020). Despite this, few studies applied a Q/ToF-

111 ACSM or AMS in SCB. The responses of aerosol chemistry to meteorology and emissions therein

112 remained poorly understood. To the authors' best knowledge, this is the first time that the ToF-

113 ACSM has been deployed in the field observations within SCB.

114   The present study aims to uncover the factors driving severe haze formation during winter in

115 SBC. The characteristics of NR-$PM_{2.5}$, including mass concentration, chemical composition,

116 temporal and diurnal variation, were described in detail. The OA sources resolved by the positive

117 matrix factorisation (PMF) analysis and elemental composition were investigated to elucidate the

118 possible aging process of OA. The formation mechanism for SIA and SOA was also studied based

119 on the dependencies of nitrate, sulphate and OOA with odd oxygen ($Ox = O_3 + NO_2$) and aerosol

120 liquid water content. In addition, the evolution process of chemical composition and elemental

121 composition were summarised during different haze and fog episodes to investigate the main factors

122 exacerbating haze pollution. The data and results would fill the knowledge gap on the factors

123 affecting haze formation in SCB and provide a scientific basis for future air pollutant mitigation

124 strategies in this unique basin.

125 **2. Material and methods**

126 **2.1 Sampling site**

127   The field study was carried out from 18 December 2021 to 22 January 2022 at a site (30°55'59"

128 N, 104°12'25"E) in Deyang, and the site was near the northern border of Chengdu, the capital of

129 Sichuan province, China (as shown in Fig. 1). The site was located in a typical suburban region

130 surrounded by several food, aluminium alloy, and building materials factories. There was a main

131 road ~200 m south of the site. The north and west of the site were croplands and villages. Thus, the

132 site was affected by traffic emissions, biomass burning and industrial pollutants. The study at this

133 site would help to understand the characteristics of regional haze pollution and the influence of

134   regional transport between urban and suburban areas on haze formation

2.2 Instrumentation

135

136   During the campaign, the mass loadings of non-refractory organics, nitrate, sulphate,

137   ammonium and chloride in $PM_{2.5}$ were obtained online by a ToF-ACSM. The gaseous species,

138   including NO, NO_2, O_3, SO_2, CO and CO_2, were continuously measured by the Thermo gas

139   analysers (model 43i, 49i, 42i, 48i and 410i). The meteorological parameters, including temperature

140   (T), relative humidity (RH), solar radiation (SR), wind speed (WS) and wind direction (WD), were

141   obtained by an automatic weather station (Luff WS501-UMB).

142   For the NR-$PM_{2.5}$ measurement, the ambient air was pumped into the sampling line via a

143   vacuum pump, and the flow rate was maintained at 3 L/min with a ~~flow meter~~ mass flow controller.

144   Before being sampled by the ToF-ACSM, the ambient air would go through a $PM_{2.5}$ cyclone (URG-

145   2000-30ED, USA) to remove coarse particles, then was dried by a Nafion drier. The relative

146   humidity of the air samples dried by the Nafion drier usually ranged from ~35% to 46 %, and could

147   reach ~56 % during fog events. The sampling line was assembled using 3/8' stainless steel tubes

148   coated with the sponge to prevent water condensation.

149   The working principle of ToF-ACSM had been described in detail in previous studies (Ng et

150   al., 2011; Fröhlich et al., 2013). Briefly, a 100 μm critical orifice and an aerodynamic lens were

151   settled in the front inlet system to focus the ambient particles into a concentrated and narrow beam

152   with a flow rate of ~0.084 L/min. It should be mentioned that a $PM_{2.5}$ lens was used during the

153   whole campaign, which allowed to chemically characterise the $PM_{2.5}$ composition ~~which made the~~

154   ~~$PM_{2.5}$ measurement available~~ (Xu et al., 2017).

155   The particle beam was transmitted through a vacuum chamber in which the gas-phase species

156   were separated from the particle beam. At the end of the vacuum chamber, the particles were

157   thermally vaporised at ~600 ℃ by impacting on a resistively heated porous tungsten surface. There

158   the non-refractory constituents in the particles flash vaporise and are subsequently ionised by a 70

159   eV electron impact. Finally, the ions were extracted by a set of ion optics and detected by the time-

160   of-flight mass spectrometer.

161   The ToF-ACSM was operated with a time resolution of 10 mins and scanned from m/z 10 to

219. The ionisation efficiency (IE) calibration was performed before and after the campaign

according to the proposal of a previous study (Fröhlich et al., 2013). Briefly, the size-selected (350

nm) NH_4NO_3 particles, which were generated by an aerosol generator, were simultaneously sampled

by the ToF-ACSM and a condensation particle counter (CPC 3775, TSI). Then, the IE can be

determined by comparing the response of ToF-ACSM to the mass of ammonium nitrate. The relative

ionisation efficiencies (RIEs) of sulphate and ammonium were also determined by sampling

$(NH_4)_2SO_4$ particles.

2.3 Data process

2.3.1 ToF-ACSM data analysis

The ToF-ACSM data analysis software (Tofware v2.5.13) written in Igor (Wavemetrics, Lake

Oswego, OR, USA) was used to analyse the mass concentration and chemical composition. The IE

value was 239 ions/pg, and the RIEs for sulphate and ammonium were 1.05 and 3.6, respectively.

For organics, nitrate and chloride, commonly used RIE values, i.e. 1.4, 1.1 and 1.3, were applied.

The algorithm proposed by Middlebrook et al. (2012) to determine the collection efficiency (CE) of

ToF-ACSM was applied to quantify the aerosol species, as the acidity, chemical composition, and

phase state changed the particle bounce effects at the vaporiser (Matthew et al., 2008).

The triangle plot of $f44$ (ratio of m/z 44 to total signal in the component mass spectrum) versus

$f43$ (ratio of m/z 43 to total signal in the component mass spectrum) and $f44$ versus $f60$ (ratio of m/z

60 to total signal in the component mass spectrum) were applied to characterise the evolution of OA

(Ng et al., 2010). The O/C and H/C were determined by the parameterization proposed by

Canagaratna et al. (2015).

2.3.2 PMF analysis

The mass spectrum data matrix of OA was analysed by the PMF Evaluation Tool (PET, v2.08D)

(Paatero and Tapper, 1994; Ulbrich et al., 2009) in order to resolve distinct OA factors that might

be representative of specific sources. The PMF-ACSM data processing was followed by the

procedures proposed previously (Ulbrich et al., 2009; Zhang et al., 2011). Due to the weak signal

188 intensities, the ions with m/z over 120 were not included in the analysis. Any ions with signal-to-

189 noise (S/N) < 0.2 were removed from the analysis, and the ions whose S/N was 0.2–2 were down-

190 weighted by increasing their errors calculations by a factor of 2 (Sun et al., 2011). Different PMF

191 solutions were resolved by varying the factor number from 2 to 7. The solutions were evaluated by

192 comparing the mass spectral profiles of the output secondary aerosol factors as a function of the

193 rotational parameter (fpeak). Finally, a three-factor solution with fpeak = 0 was selected as our best

194 solution. The comparison of the results for three to five-factor solutions was described in detail in

195 Fig. S4 and Table. S2.

196 **2.3.3 Identification of haze episodes**

197 The haze episodes were defined by the daily $PM_{2.5}$ mass concentration exceeding Grade II

198 National Ambient Air Quality Standard (AAQS) of 75 $\mu g/m^3$ for two successive days (Wang et al.,

199 2014). In the present study, we made some slight modifications to this definition following the

200 procedure of Zheng et al. (2016). Briefly, the periods during which the 24 h-moving average

201 concentration of $PM_{2.5}$ exceeds 75 $\mu g/m^3$ for two successive days are regarded as episode candidates.

202 If the hourly $PM_{2.5}$ concentration during the first hour of an episode candidate is 50-75 $\mu g/m^3$, then

203 the episode has a shape of 'slow start'; if it is 0-50 $\mu g/m^3$, then the episode has the shape of the 'rapid

204 start'. Similarly, the shape at the end of an episode candidate can also be identified. Haze episodes

205 having a 'slow start' typically arise from the gradual accumulation of pollutants emitted both locally

206 and regionally under unfavourable meteorological conditions, while haze episodes having a 'rapid

207 start' are most likely related to regional transport (Zheng et al., 2015). Haze episodes having a 'slow

208 end' usually resulted from the gradual scavenge of pollutants.

209 According to the definition mentioned above, three haze episodes (denoted as H1, H2 and H3,

210 respectively, in Fig. 2), all with the types of 'slow start' and 'slow end', were identified over the whole

211 campaign. In addition, a fog event occurred during each haze episode (denoted as F1, F2 and F3,

212 respectively). Lacking the information of visibility and aerosol size distribution up to several tens

213 of micrometres, we were not able to precisely diagnose the accumulation and dissipation stages of

214 a fog event. Instead, we selected the hours with RH near 100 % as the duration of a fog event, which

215 was the same as the condition described in previous studies (Izhar et al., 2020; Guo et al., 2015).

2.4 Air parcels trajectories analysis

216

217   2-day back trajectories arriving at the receptor site were calculated every hour over the whole

218 campaign using the National Oceanic and Atmospheric Administration (NOAA) HYSPLIT version

219 4 (Draxler and Hess, 1998). Input to the model is in the form of $1°$ latitude-longitude gridded

220 meteorological parameters from the Global Data Assimilation System meteorological dataset. We

221 chose an arrival height of 500 m which is above ground level (AGL) for target analysis in the

222 HYSPLIT model to diminish the effects of surface friction (Polissar et al., 2001); this height value

223 and greater are regarded as in the open height of the planetary boundary layer in winter and are more

224 useful for long-range transport. Finally, 839 backward trajectories in total were obtained. Then,

225 these trajectories were grouped into four clusters, i.e., cluster 1 from the north, cluster 2 from the

226 southwest, cluster 3 from the northeast, and cluster 4 from the east. The trajectories of each cluster

227 accounted for 12.6, 6.2, 58.4, and 22.8 % of total air parcels trajectories during the whole campaign,

228 respectively.

3. Results and discuss

229

3.1 Overview of meteorology and PM$_{2.5}$ chemical composition

230

231   The temporal variation of meteorological parameters, concentrations of gaseous pollutants, and

232 chemical compositions of PM$_{2.5}$ over the whole campaign are illustrated in Fig. 2. The missing data

233 were due to the acquisition software malfunction of the instrument. During the campaign, the

234 temperature ranged from -1.9 to 16.3 ℃ with a mean value of 7.3 $\pm$ 2.8 ℃, and the RH ranged from

235 35 to 100 % with an average of 81 $\pm$ 12.4%. The wind from the southwest prevailed with an average

236 speed of 0.7 $\pm$ 0.5 m/s during the entire campaign. This indicated that the atmosphere was in a

237 stagnant state with relatively low temperature and high RH.

238   The mass concentration of NR-PM$_{2.5}$ during the campaign ranged from 23 to 230 μg/m^3, with

239 an average of 98.5 $\pm$ 38.7 μg/m^3. This was comparable to the average PM$_{2.5}$ concentrations during

240 wintertime in other cities in the SCB (Table S1). The OA concentration varied from several to 103

241 μg/m^3, with an average of 39.2 $\pm$ 3.9 μg/m^3, constituting the majority of PM$_{2.5}$. OA contributed ~20-

242 69 % to PM$_{2.5}$ with an average of 40.3 $\pm$ 7.6 %. The average concentrations of nitrate, sulphate,

243   ammonium and chloride were 29 ± 14 (ranging from ~4 to 80 μg/m³), 10 ±4.2 (ranging from ~2 to

244   28 μg/m³), 15.1 ± 6.4 (ranging from ~3 to 38 μg/m³) and 5.2 ±4.1 μg/m³ (ranging from ~1 to 50

245   μg/m³), taking up 28.8 ± 5.5, 10.6 ± 2.8, 15.3 ± 2.2 and 5.1 ± 3.1 % of PM$_{2.5}$, respectively. The

246   dominance of organic species was similar to previous observations in urban Chengdu during the

247   winter of 2014 and 2015 (Kong et al., 2020; Wang et al., 2018). However, the nitrate concentration

248   was higher than that of sulphate, which was contrary to that reported previously. A recent

249   observation in urban Chengdu also found that higher fraction of nitrate in PM$_{2.5}$ compared to

250   sulphate, probably due to the remarkable decrease in SO$_2$ emission in the past ten years (Huang et

251   al., 2021; Fu et al., 2017).

3.2 Characteristics of inorganic aerosol

253   The correlation between the molar equivalent concentrations of measured ammonium and the

254   sum of molar equivalent concentrations of nitrate, sulphate and chloride was illustrated in Fig. 3.

255   The slope of the regression line for ammonium against the sum of nitrate, sulphate and chloride with

256   a value of 1.01 indicated that the anions in PM$_{2.5}$ were well neutralised by cation (ammonium). This

257   result illustrated that nitrate, sulphate, and chloride were mainly in the form of NH$_4$NO$_3$, (NH$_4$)$_2$SO$_4$

258   and NH$_4$Cl, which were commonly considered secondarily formed (Ianniello et al., 2011; Ge et al.,

259   2017).

260   As SO$_4^{2-}$ competed with NO$_3^-$ for NH$_4^+$ during their formation, the relationship between nitrate-

261   to-sulphate molar ratio ([NO$_3^-$]/[SO$_4^{2-}$]) and ammonium-to-sulphate molar ratio ([NH$_4^+$]/[SO$_4^{2-}$])

262   was indicative of the pathway of nitrate formation (He et al., 2012). If [NO$_3^-$]/[SO$_4^{2-}$] linearly

263   correlated with [NH$_4^+$]/[SO$_4^{2-}$] under ammonium-rich conditions ([NO$_3^-$]/[SO$_4^{2-}$] $\geq$ 1.5), the

264   homogeneous formation of nitrate was expected:

$$HNO_3\ (g) + NH_3\ (g) \leftrightarrow NH_4NO_3\ (s, aq) \quad (1)$$
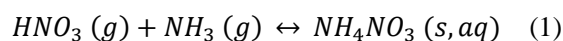
266   While for ammonium-poor conditions ([NO$_3^-$]/[SO$_4^{2-}$] < 1.5), the high concentration of nitrate

267   was attributed to its formation through hydrolysis of N$_2$O$_5$ on the pre-existing aerosols (Pathak et

268   al., 2009):

$$N_2O_5\ (aq) + H_2O\ (aq) \leftrightarrow 2NO_3^-\ (aq) + 2H^+\ (aq) \quad (2)$$
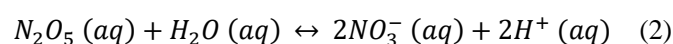
270   To better elucidate the factors affecting nitrate formation, we divided the observation period

271 into daytime (6:00 - 18:00, local time) and nighttime (18:00 - 6:00 next day, local time) hours. Fig.

272 S1 showed that the $[NO_3^-]/[SO_4^{2-}]$ during daytime was larger than 1.5, indicating ammonium-rich

273 conditions. $[NO_3^-]/[SO_4^{2-}]$ was significantly correlated with $[NH_4^+]/[SO_4^{2-}]$ during daytime with the

274 regression function:

275 $$\frac{NO_3^-}{SO_4^{2-}} = 0.69 \times \frac{NH_4^+}{SO_4^{2-}} - 1.08 \quad (3)$$

276   The intercept of the regression line on the $[NH_4^+]/[SO_4^{2-}]$ axis was 1.56, which was close to

277 1.5, as suggested by Pathak et al. (2009), implying that the nitrate formation was mainly driven by

278 the homogeneous pathway (Sun et al., 2011). Indeed, the nitrate concentration and nitrogen

279 oxidation ratio (NOR = $n(NO_3^-)/[n(NO_2) + n(NO_3^-)]$) increased as the Ox concentration increased

280 (as shown in Fig. 4), and exhibited a strong O_3/Ox ratio dependency, which further demonstrated

281 the homogeneous daytime formation of nitrate.

282   The emission of NOx and SO_2 had been reduced while NH_3 increased in the past almost ten

283 years, which resulted in the ammonium-rich condition in the atmosphere (Fu et al., 2017; Liu et al.,

284 2018). Despite this, a recent study showed that the nocturnal nitrate formation was not sensitive to

285 NH_3, and even increased slightly as NH_3 decreased, which was likely due to the aerosol acidity

286 effects on the partitioning of nitrate (Wen et al., 2018). Thus, the fitting of $[NO_3^-]/[SO_4^{2-}]$ vs.

287 $[NH_4^+]/[SO_4^{2-}]$ might not be applicable for identifying the nitrate formation process during

288 nighttime. The average O_3 concentration was 13.7 μg/m^3 and the average RH was 83.3 % during

289 nighttime, which favoured the aqueous-phase reactions to occur. Higher nitrate concentration was

290 observed with increasing ALWC during nighttime (as illustrated in Fig. S2), and so was NOR. This

291 phenomenon further implies the heterogeneous hydrolysis of N_2O_5 might dominate the formation

292 of nocturnal nitrate. The results were consistent with the study of Tian et al. (2019), which showed

293 that heterogeneous hydrolysis of N_2O_5 dominated nitrate formation during nighttime, while

294 photochemical reactions also played an important role in nitrate formation during daytime in two

295 megacities in Sichuan Basin.

296   Fig. S2(a) showed that the average sulphate concentration increased slightly when Ox > 60

297 μg/m^3 during daytime hours, suggesting the contribution of the photochemical process to sulphate

298 formation. However, the overall sulphur oxidation ratio (SOR = $n(SO_4^{2-})/[n(SO_2) + n(SO_4^{2-})]$)

299 decreased with increasing Ox (Fig. 4(b)), suggesting the photooxidation was not efficient for

300 converting SO_2 to sulphate. By contrast, SOR showed an increasing trend as ALWC increased,

301 demonstrating the efficient conversion of SO_2 to sulphate through aqueous-phase reactions. A

302 previous study showed that the aqueous oxidation of SO_2 by NO_2 is key to efficient sulphate

303 formation on fine aerosols with high relative humidity and NH_3 neutralisation (Wang et al., 2016).

304 As mentioned above, the atmospheric aerosols were well neutralised, and RH was high, which

305 favoured the following reaction to occur:

306 $$SO_2 \ (g) + 2NO_2 \ (g) + \ 2H_2O \ (aq) \rightarrow 2H^+(aq) + \ SO_4^{2-}(aq) + \ 2HONO(g) \quad (5)$$
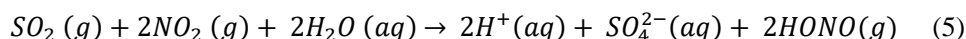
3.3 Characteristics of organic aerosol

3.3.1 Source appointment of OA

309 PMF analysis was performed to explore the OA sources measured during the whole campaign.

310 A three-factor solution was chosen as the best PMF analysis results based on the mass spectra profile,

311 variation of Q/Qexp, diurnal variation and correlation with external tracers. The resolved factors

312 included a hydrocarbon-like OA (HOA), a biomass burning OA (BBOA) and an oxygenated OA

313 (OOA). The mass spectra profiles of these three factors were shown in Fig. 5, and the temporal

314 profile of each factor and its external tracer were also shown.

315 The mass spectrum of HOA was dominated by the ions of m/z 29, 41, 55, 57, 69 and 71. HOA

316 was well correlated with BC (r = 0.77), which was largely emitted by vehicles. The diurnal cycles

317 of HOA showed two peaks during typical rush hours, demonstrating the contribution of traffic

318 emissions to HOA (Lanz et al., 2007; Zhang et al., 2005). The average concentration of HOA was

319 $8.9 \pm 6.5 \ \mu g/m^3$ and constituted $24.2 \pm 10.4 \ \%$ of OA over the whole campaign. The increased

320 fraction of HOA as a function of total OA (Fig. 6) demonstrated the contribution of motor vehicle

321 emissions to haze formation.

322 BBOA was characterised by the pronounced peaks at m/z 60 (mainly $C_2H_4O_2^+$) and 73

323 ($C_3H_5O_2^+$), which were generally regarded as biomass burning markers from levoglucosan

324 compounds (Mohr et al., 2012; Weimer et al., 2008; Alfarra et al., 2007). BBOA was well correlated

325 with m/z 60 and m/z 73 (r = 0.76 and 0.94, respectively) and accounted for 88 % of m/z 60 and 70 %

326 for m/z 73, which were higher than those in other sources. A good correlation was also found

327 between BBOA and chloride (r = 0.64), which was also suggested to be one of the tracers of biomass

328 burning. The diurnal variation of BBOA showed a similar trend of chloride (Fig. S3(a)), with two

329 peaks during 8:00-10:00 and at 19:00, which was due to the residential cooking and heating using

330 biomass. The concentration of BBOA ranged from ~1 to 34 $\mu g/m^3$, with an average of 8.9 $\pm$ 5.4

331 $\mu g/m^3$. BBOA took up 24.2 $\pm$ 8.6 % with a maximum of 46 % of OA, and its fraction also increased

332 with increasing total OA concentration, indicating the contributions of biomass burning activities

333 during haze episodes.

334   OOA was featured by the dominant signal intensities at m/z 28 (mainly CO^+) and m/z 44 (CO_2^+).

335 OOA accounted for 69 % of m/z 44, which was higher than those in other sources. The time series

336 of OOA correlated well with those of nitrate and sulphate (r = 0.81 and 0.72, respectively),

337 suggesting the commonly regional and aged properties of OOA. The concentration of OOA

338 accumulated gradually from 8:00 to 13:00, then decreased till night time. The diurnal cycle of OOA

339 was similar to solar radiation (as shown in Fig. S3(d)), suggesting OOA formation was associated

340 with photochemical reactions. The average OOA concentration showed increasing trends as Ox

341 concentration increased during both daytime and nighttime (Fig. S5), indicating the probable

342 formation pathways of OOA from its precursors (Kuang et al., 2020; Zhan et al., 2021). Note that

343 the accumulation of NO_2 would lead to the decrease of O_3/Ox ratio at night; thus, Ox might not be

344 an appropriate indicator of photochemical oxidation (Xu et al., 2017; Herndon et al., 2008). The

345 OOA formation might be attributed to other processes during nighttime. For example, previous

346 studies showed that high NOx concentration facilitated the formation of nitrate radical (NO_3), and

347 the NO_3 oxidation of biogenic volatile organic compounds (BVOC) was important for nighttime

348 secondary organic aerosol formation (Boyd et al., 2017; Rollins et al., 2012). Except that the

349 average OOA concentration showed an increasing trend when ALWC < 200 $\mu g/m^3$ during nighttime,

350 OOA concentration did not change significantly with increasing ALWC during both day- and

351 nighttime, suggesting the aqueous-phase reactions were not a significant pathway toward OOA

352 formation.

353 **3.3.2 Elemental composition of OA**

354   The f44 vs. f43 and f44 vs. f60 during the entire campaign were illustrated in Fig. 7. The triangle

plot of $f44$ vs. $f43$ has been widely used to characterise OA evolution in the atmosphere because m/z's 44 and 43 are usually from different functional groups, and the ratio changes as a function of atmospheric aging. The $f43$ ranged from ~0.06 to 0.12 with an average of 0.08 ± 0.009, and the range of $f44$ was ~0.07-0.24 with an average of 0.15 ± 0.03, suggesting the existence of both fresh and aged aerosols in the atmosphere. Most of the data were within the triangle space characterised by a series of field observations and experimental data (Ng et al., 2011). However, those points with higher $f44$ were outside the upper boundary of the triangle region, suggesting the corresponding aerosols were more oxidised. It could be observed that the points with higher $f44$ (> 0.16) corresponded to relatively higher Ox concentration and lower ALWC, while those with lower $f44$ corresponded to relatively lower Ox concentration and higher ALWC, suggesting that the formation of more oxidised OOA was mainly attributed to photochemical reactions, and the formation of less oxidised OOA was probably attributed to aqueous-phase reactions (Zhao et al., 2019; Kim et al., 2019).

The triangle plot of $f44$ vs. $f60$ was widely used as a metric to access the evolution of atmospheric BBOA (Cubison et al., 2011). A value of 0.003 for $f60$ was recommended as an appropriate value to represent the atmospheric background free of biomass burning influence (Aiken et al., 2009; Docherty et al., 2008). The $f60$ ranged from 0.0028 to 0.055 with an average of 0.008 ± 0.003 during the campaign. Except for several points, the $f60$ was ubiquitously higher than 0.003 and most points fell in the triangular region, suggesting the contribution of biomass burning to OA. The $f44$ and $f60$ of BBOA resolved by PMF in the present study were also in the triangular region and comparable with previous studies (Paglione et al., 2020; Zhao et al., 2019; Kim et al., 2019). Fig. S6 showed that $f44$ increased while $f60$ decreased with increasing Ox, indicating the likely oxidation of levoglucosan and/or levoglucosan-like substances. Cubison et al. (2011) suggested that the increasing $f44$ was not only attributed to the oxidation of levoglucosan-like species, but the oxidation of bulk OA also played a role because the levoglucosan-like species only contributed a small fraction of the OA mass (Aiken et al., 2009). Their contribution to the total signal m/z 44 before or after aging was also small. Compared to the effects of Ox, the increasing ALWC did not seem to push $f60$ to the left upper region. Most of the data points, which corresponded to high ALWC, were within the region of aged BBOA in the $f44$ vs. $f60$ space as defined previously by Paglione et al. (2020), indicating the probable aqueous-phase oxidation of BBOA. Although the

385 aqueous OOA (aq-OOA) could not be resolved in the present study, we deduced that the aqueous-

386 phase reactions occurred and contributed to the formation of OOA, for (1) the ambient RH was

387 typically above 65%, which favoured the presence of wet aerosol particles; (2) the range of O/C

388 estimated from the Improved-Ambient (IA) method varied from 0.46 to 0.85 when the ambient RH $>$

389 80 %, covering the O/C range of the OOA obtained from the photooxidation of organic precursors

390 in the aqueous phase and ambient aq-OOA observed in many other cities (Duan et al., 2021;

391 Mandariya et al., 2019; Sun et al., 2010; Xu et al., 2017; Gilardoni et al., 2016).

392 The evolution of OA during the whole campaign was characterised by the van Krevelen (VK)

393 diagram in Fig. 8. The slope obtained from the linear regression of H:C versus O:C plotted in the

394 VK-$\overline{OS_c}$ space could be used to infer the composition of OA and the chemical process in OA

395 formation (Docherty et al., 2018). The slope of 0 in VK-$\overline{OS_c}$ plot was related to the replacement of

396 a hydrogen atom with an OH moiety, while the slopes of -0.5 and -1 indicated the formation of

397 carboxylic groups with/without fragmentation, and a slope of -2 was equivalent to the replacement

398 of an aliphatic carbon with a carbonyl group (Heald et al., 2010; Ng et al., 2011). The slope of the

399 linear fitting line for all the data points was -0.14, suggesting the probable formation of carboxylic

400 acid moieties and hydroxyl groups. The slopes of the linear fitting lines for each fog episode were similar

401 and close to zero, which was consistent with the hydroxyl group formation possibly taking place in

402 aerosol water through dark chemistry (Sun et al., 2010; Yu et al., 2014; Zhao et al., 2014).

403 **3.4 Regional transport**

404 Air parcels from the north (cluster 1) transported at relatively high heights before arriving at

405 the observation site (as illustrated in Fig. 9), and corresponded to the lowest average $PM_{2.5}$

406 concentration ($66 \pm 30\ \mu g/m^3$). The air parcels of cluster 2 Clsuter2 had the longest transport distance

407 and highest transport height. Although they took up the least proportion of total air parcels, they had

408 the highest average $PM_{2.5}$ concentration ($119 \pm 30\ \mu g/m^3$) during the whole campaign, suggesting

409 that pollutants accumulated high in the air. Air parcels from the east (cluster 3) with the shortest

410 transport distance and relatively low transport height had an average $PM_{2.5}$ concentration of $113 \pm$

411 $34\ \mu g/m^3$. This indicated that the pollutants might be brought to the observation site along with the

412 transport of air parcels originating from adjacent areas. The air parcels from the northeast of Sichuan

413   province (cluster 4) had the lowest transport height; however, the corresponding $PM_{2.5}$ concentration

414   was lower than that of cluster 3.

415   Compared to cluster 1 and cluster 4, a higher contribution of nitrate to $PM_{2.5}$ was observed for

416   cluster 2 and cluster 3, which was mainly related to the intense emission from industry and vehicles.

417   However, the contribution of BBOA was higher for cluster 3 and cluster 4 compared to other clusters,

418   suggesting intense biomass burning along their transport paths.

419   To better understand the potential pollutant sources during the campaign, the potential source

420   contribution function (PSCF) was applied to analyse the possible regions that might contribute to

421   haze formation. The spatial distribution of weighted PSCF for different chemical compositions was

422   illustrated in Fig. 10. The WPSCF values for organics over the southwest and southeast were > 0.7,

423   indicating these locations were likely source areas of organics. For nitrate and sulphate, the areas

424   by the southwest and south of the sampling site were potential source regions. The major source

425   regions for HOA were the areas of south and northeast Deyang. The regions contributing to BBOA

426   were the areas of east Sichuan province, which was consistent with a higher proportion of BBOA in

427    $PM_{2.5}$ in the air parcels stemming from these locations. For OOA, the WPSCF values over the

428   southwest and southeast of Deyang and northeast Sichuan province were > 0.7, suggesting the

429   contribution of these regions.

430   **3.5 Case studies for haze pollution**

431   **3.5.1 Factors driving the evolution of haze episodes**

432   As mentioned above, three haze episodes were identified over the whole campaign. The

433   synoptic conditions and aerosol chemical composition for each haze episode were summarised in

434   Table. S3. The average temperature during H2 was lower than those during H1 and H3, while the

435   average solar radiation was higher. The mean RH and wind speed were almost the same during each

436   haze episode. The average concentrations of aerosol chemical composition and their contributions

437   to $PM_{2.5}$ were different in each haze episode, indicating that the factors causing haze formation

438   might be different during the campaign.

439   The average $PM_{2.5}$ concentrations measured by ToF-ACSM during H1, H2, and H3 were 113

440   ±46, 109 ±46, and 104 ± 30 µg/m³, respectively. The average mass fractions of OA, nitrate, sulphate,

441 ammonium, and chloride were similar during H1 and H3 (as shown in Fig. 11(a)). During H2, the

442 mass fractions of sulphate and ammonium were slightly higher than those in H1 and H3, while the

443 mass fractions of OA and chloride were lower. In OA, the fraction of primary organic aerosols (POA

444 = HOA + BBOA) during H3 was higher than those during H1 and H2. The fraction of BBOA showed

445 an increasing trend from H1 to H3, demonstrating the contribution of biomass burning to haze

446 formation. Despite the importance of BBOA to winter haze formation in SCB, the control of biomass

447 burning did not receive much attention, and more efforts were needed for atmospheric aerosol

448 mitigation in the future.

449 Fig. 11(b) showed that the concentrations of OA, nitrate, sulphate, ammonium, and chloride

450 all increased as the ambient air quality worsened (implying by the increasing $PM_{2.5}$ concentration)

451 during each haze episode. During H1, the fraction of nitrate in $PM_{2.5}$ increased, while the proportions

452 of sulphate, OOA, and HOA in $PM_{2.5}$ decreased as the $PM_{2.5}$ concentration increased, indicating the

453 evolution of this haze episode was mainly driven by the reactions involving nitrate formation. The

454 average NO_3^- formation rate as a function of $PM_{2.5}$ concentration during H1 was depicted in Fig. S7.

455 The NO_3^- formation rate increased fast as $PM_{2.5}$ concentration increased from 50 to 110 $\mu g/m^3$,

456 which also showed the rapid formation of nitrate contributed to haze formation. In contrast, the

457 average nitrate formation rates were below zero when the $PM_{2.5}$ concentration was < 130 $\mu g/m^3$

458 during H2 and H3, suggesting nitrate formation did not play an important role at the early stage of

459 H2 and H3. Although the nitrate formation rate decreased when $PM_{2.5}$ concentration was > 110

460 $\mu g/m^3$ during H1, it remained positive, suggesting the nitrate concentration increased gradually.

461 For H2, the fraction of nitrate and ammonium in $PM_{2.5}$ did not show apparent changes, and the

462 fractions of sulphate and OOA decreased, while the fractions of BBOA and HOA increased as the

463 air quality worsened, demonstrating that the emission of primary organic aerosols from biomass

464 burning and vehicle exhaust were the major factors which drove the haze formation. ~~During H3, the~~

465 ~~fractions of nitrate and BBOA in $PM_{2.5}$ increased, while OOA decreased and the rest composition~~

466 ~~did not change significantly as the $PM_{2.5}$ concentration increased~~ During H3, the fractions of nitrate

467 and BBOA in $PM_{2.5}$ increased, while OOA decreased and HOA, sulphate, ammonium, chloride did

468 not change significantly as the $PM_{2.5}$ concentration increased, showing that the evolution of this

469 haze episode was mainly driven by the reactions involving nitrate formation and biomass burning.

470 The fire maps (as illustrated in Fig. S8) showed that more fire spots during H2 and H3 were observed

471   around Deyang compared to non-haze episodes, suggesting the biomass burning activities were

472   more intensive during these haze episodes.

473   The average estimated O:C and H:C during H1 and H2 were similar and slightly higher/lower

474   than that during H3, thus resulting in a higher carbon oxidation state ($\overline{OS_c} \approx$ 2O:C - H:C) during

475   H1 and H2. The lower average $\overline{OS_c}$ during H3 might be due to the higher proportion of HOA and

476   BBOA, which did not undergo long-time aging and kept relatively fresh in the atmosphere.

477   **3.5.2 Evolution of chemical composition during fog periods**

478   The fog periods usually started at night or early morning and dissipated in the afternoon. The

479   individual meteorological parameter differed among each fog period (as summarised in Table S3).

480   The average temperature was the highest during F1 (6.2 $\pm$ 2.3 ℃), and the lowest was observed

481   during F2 (1.5 $\pm$ 3.2 ℃). The maximum solar radiation during F1 and F2 (470 and 500 W/m^2) were

482   similar and much higher than that during F3 (75 W/m^2). The synoptic conditions with low

483   temperature and calm wind favoured the formation of radiation fogs in each fog period.

484   The chemical composition of PM$_{2.5}$ was also different during each fog period. The average

485   concentrations of organics, nitrate, and ammonium were almost the same during F2 and F3 and

486   significantly lower than those during F1. However, the average chloride concentration during F2

487   was twice of those during F1 and F3, suggesting the possibility of stronger biomass burning

488   emissions during F2. OOA constituted the major part of OA during F1, while HOA and BBOA were

489   more important than OOA during F2 and F3. The domination of secondary species in PM$_{2.5}$ during

490   F1 was probably due to the aqueous-phase reactions, while the primary emission tended to be

491   stronger during F2 and F3.

492   Since the aerosols were dried by a Nafion drier, the aerosols that ToF-ACSM measured were

493   the interstitial particles in droplets or those excluded from fog droplets. In order to better characterise

494   the evolution of chemical composition in each fog period, the intervals for 3 h before and after the

495   fog period, when ambient RH was lower than 95 %, were regarded as pre-fog and post-fog periods,

496   respectively (Kim et al., 2019). Note that the post-fog was not assigned for F3 because the ToF-

497   ACSM data were not available with a failure of acquisition software.

498   The average concentrations of different chemical compositions during the evolution of fog

episodes (pre-fog, during fog, and post-fog) were illustrated in Fig. 12. Compared to the pre-fog period of F1, all species in the interstitial aerosols decreased during the foggy period, likely due to the scavenging by fog droplets. Note that the OOA and sulphate decreased less than other species, probably due to the OOA and sulphate formation through aqueous-phase reactions against the scavenging effect of fog droplets. Except for OOA and nitrate, all species kept decreasing during post-fog periods, which might be attributed to the increase of the planet boundary layer (PBL) height. The increase of OOA and nitrate was probably associated with the enhancement of photochemical reaction after the dissipation of fog.

~~Distinguished from F1, all species (except for HOA) increased during the foggy period from the pre-fog period during F2~~ All species (except for HOA) increased during the foggy period from the pre-fog period during F2, which was different from the case during F1. Although hydrophilic species (e.g., nitrate, sulphate, and OOA) tended to be scavenged by fog droplets, it seemed that the formation of OOA, nitrate, sulphate, and ammonium was significantly faster than wet removal, thus resulting in an increase during the foggy period. BBOA and HOA were commonly considered as hydrophobic species, and they were excluded from fog droplets. Previous studies showed that BBOA and HOA concentrations decreased during the foggy period compared to the pre-fog period (Collett et al., 2008; Kim et al., 2019), despite their insoluble nature. ~~The increase of BBOA in the present study was attributed to the intense emission from biomass burning during the foggy period, which overwhelmed the scavenging effects of fog droplets.~~ The increase of BBOA in the present study was likely attributed to the intense emission from biomass burning during the foggy period, which overwhelmed the scavenging effects of fog droplets. The enhanced partitioning of biomass burning VOCs under high RH conditions might also contribute the increase of BBOA. For example, a recent study showed that the large quantities of phenols from biomass burning emission would readily partition into the atmospheric aqueous phase (Xiao et al., 2022). During the post-fog period, BBOA and HOA decreased significantly, possibly due to weaker emission and the efficient removal of fog droplets through nucleation and/or coagulation. The dynamics of PBL might also play a role because the temperature kept increasing, and higher PBL was expected during the post-fog period. With stronger solar radiation, OOA, nitrate, and ammonium continued growing during the post-fog period from the foggy period through photochemical reactions. However, sulphate slightly decreased, which might be due to the insufficient formation through photochemical reactions, and

529   decreased as the PBL height increased. Similar to F2, all the secondary species increased during the

530   foggy period from the pre-fog period during F3. However, BBOA and HOA were reduced

531   significantly by the scavenging of fog droplets and/or by the conversion to OOA through aqueous

532   phase reactions.

533   The average elemental O:C showed an increasing trend from pre-fog periods to post-fog/foggy

534   periods, while H:C did not change significantly for different fog events, suggesting the OA became

535   more oxidised. As shown in Fig. S9, the mass fractions of OOA increased, while the contribution

536   of BBOA and HOA decreased from pre-fog periods to post-fog/foggy periods for the three fog

537   events. Except for the scavenging of fog droplets, BBOA and HOA could also be oxidised to OOA

538   through aqueous-phase reactions (Wang et al., 2021), thus resulting in the decrease contribution of

539   BBOA and HOA. ~~As shown in Fig. S9, the mass fractions of OOA increased, while the contribution~~

540   ~~of BBOA and HOA decreased from pre-fog periods to post-fog/foggy periods for the three fog~~

541   ~~events.~~ As a consequence, the O:C increased in line with the increased contribution of OOA.

542   Previous studies had reported that the aqueous-phase reactions enhanced OOA formation during

543   fog/high RH periods (Chakraborty et al., 2016; Kuang et al., 2020; Chakraborty et al., 2015). It

544   appeared that the OOA formation would balance out the scavenging of fog droplets during the foggy

545   period for the three fog events, despite the hydrophilic OOA being preferentially scavenged by fog

546   droplets. Thus, the OOA concentration marginally decreased or even increased during foggy periods.

547 **4. Conclusions**

548   Haze pollution has long been a severe environmental problem in SCB. ~~The formation process~~

549   ~~of haze pollution in SCB might be different from those in NCP, YRD, and PRD due to the unique~~

550   ~~topography and meteorological conditions, which are still unclear~~ The formation process of haze

551   pollution in SCB might be different from those in NCP, YRD, and PRD due to the unique topography,

552   meteorological conditions and emission sources, which are still unclear. Based on the measurement

553   data of a ToF-ACSM and combined with the PMF and PSCF analysis, the temporal variation,

554   formation process, and sources of $PM_{2.5}$ were characterised to elucidate further the factors

555   contributing to haze formation. It was found that the concentrations of OA and nitrate increased

556   dramatically as $PM_{2.5}$ concentration increased, and the stagnant synoptic condition favoured the

accumulation of these pollutants. For different haze events, the driving factors could be classified into three types: one was the reactions involving nitrate formation; another one was the intense biomass burning and vehicle exhaust emissions, and the last one was the combination of the reactions involving nitrate formation and biomass burning. Nitrate formation was primarily affected by photooxidation during daytime, while the nocturnal nitrate formation was dominated by aqueous-phase reactions. OOA constituted a major part of OA, and it was mainly generated through photooxidation, while aqueous-phase reactions did not significantly promote its formation.

~~Due to the limitation of the present study, the parameters which are indicative of the pathways of nitrate formation are not characterised. The major precursors contributing to a large amount of OOA are not clear yet. In addition, how controlling BBOA will affect the atmospheric visibility, radiative forcing, and climate change in SCB needs further investigation in the future. In spite of the deficiencies, the results in this study implied that controlling primary emissions (such as biomass burning and vehicle exhaust) and precursors of secondary aerosols (e.g., NOx, SO$_2$, and VOCs) during severe haze periods will benefit the improvement of air quality in SCB.~~ Due to the limitation of the present study, the parameters which are indicative of the pathways of nitrate formation are not characterised. The major precursors contributing to a large amount of OOA are not clear yet. In addition, further investigation is needed to gain a better understanding of the gas/particles emitted by biomass burning or other primary emissions and how they will affect the haze formation processes, which may help to implement appropriate POA emission control to reduce the occurrence of haze. Nonetheless, the results in this study implied that controlling primary emissions (such as biomass burning and vehicle exhaust) and precursors of secondary aerosols (e.g., NOx, SO$_2$, and VOCs) during severe haze periods will benefit the improvement of air quality in SCB.

581 *Data availability.* The data generated and analysed in this study are available on visiting

582 https://doi.org/10.5281/zenodo.6965551.

583

584 *Author contributions.* FY and SX designed this study. XZ and QL contributed to data collection

585 during the field campaign. JZ, DZ, and CZ performed field experiments. ZL and CP performed the

586 data analysis. ZB wrote the manuscript. GS, LZ, and YC contributed to the scientific discussion and

587 paper correction.

588

589 *Competing interests.* The authors declare that they have no conflict of interest.

590

591 *Acknowledgements.* This work was supported by the National Key Research and Development Program of China

592 (grant no. 2018YFC0214001), and the National Natural Science Foundation of China (grant no. 42075109).

593

594 *Financial support.* This research has been supported by the National Key Research and Development Program of

595 China (grant no. 2018YFC0214001), and the National Natural Science Foundation of China (grant no. 42075109).

596
597

598
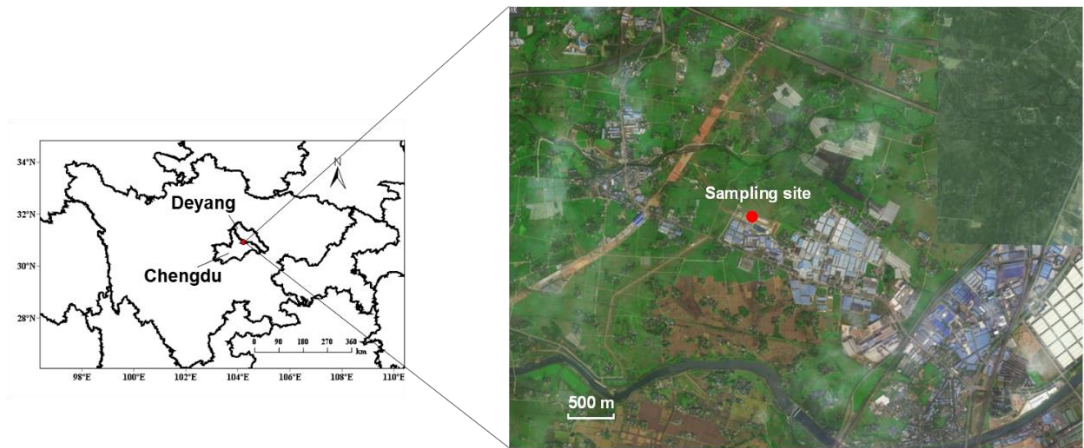
599

600   Fig. 1 Location of the observation site (from Baidu Maps, ©2022 Baidu – GS(2021)6026).

601

602

603

604
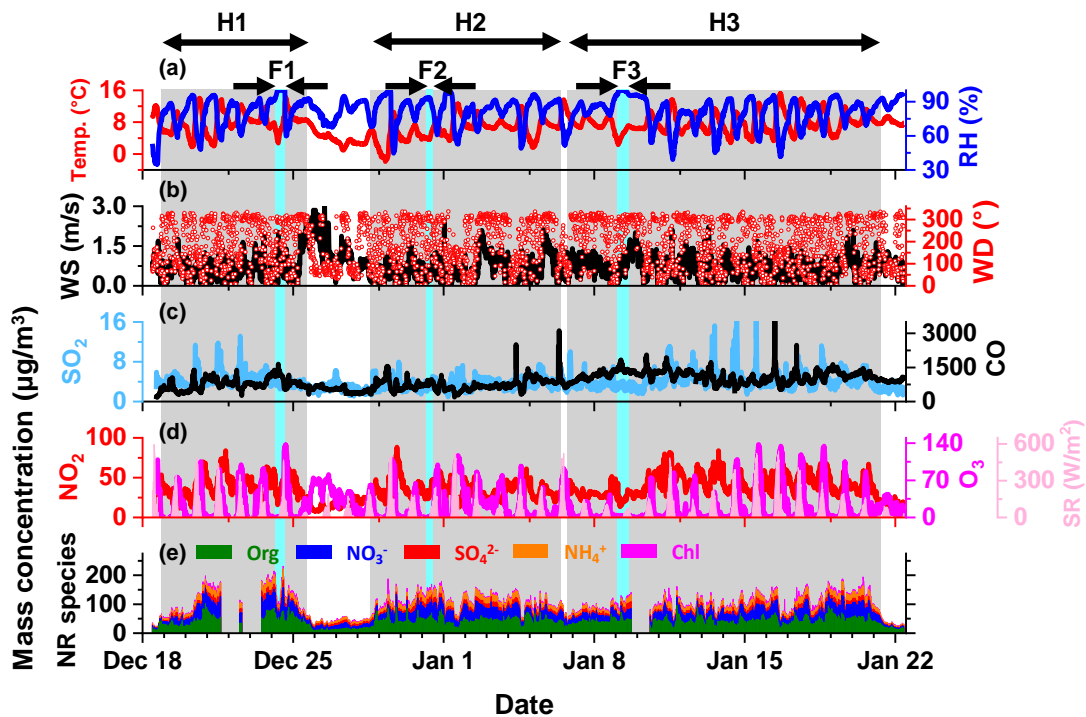
605 Fig. 2 Time series of (a) relative humidity (RH) and temperature (T); (b) wind direction and wind

606 speed; (c), (d) CO, NO_2, SO_2, and O_3 mass concentrations and solar radiation; (e) mass concentration

607 of organics, nitrate, sulphate, ammonium, and chloride in NR-$PM_{2.5}$. The grey-shaded areas

608 represent the intervals of H1, H2, and H3, respectively. The light blue-shaded areas represent the

609 intervals of F1, F2, and F3, respectively.

610

611
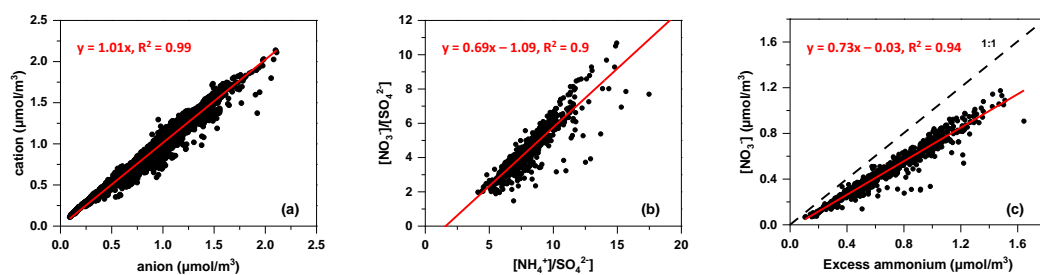
612   Fig. 3 Scatter plots of (a) molar concentrations of cations vs. anions, (b) molar ratios of nitrate to

613   sulphate vs. ammonium to sulphate, and (c) molar concentrations of nitrate vs. excess ammonium.

614

615

616

617
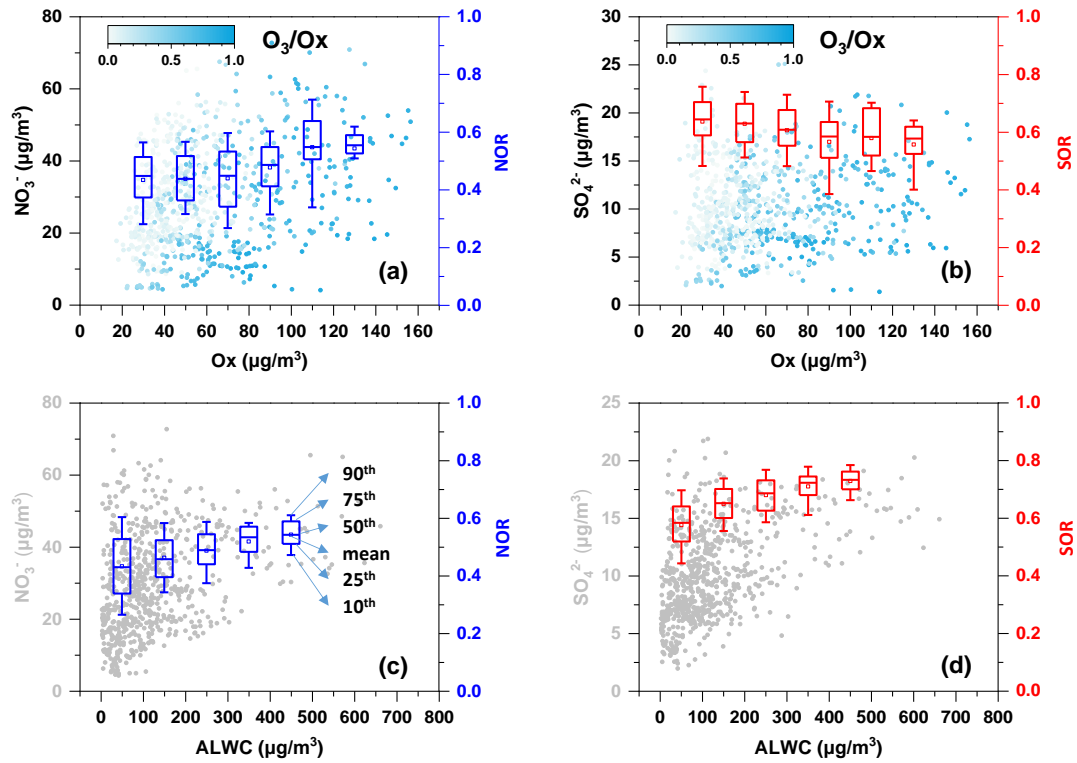
Fig. 4 Variation of (a), (c) nitrate and NOR and (b), (d) sulphate and SOR as Ox/ALWC increases.

The data NOR and SOR were grouped into different bins according to 20 μg/m³ increment of Ox in

(a) and (b), and 100 μg/m³ increment of ALWC in (c) and (d). The colour scale represents O_3/Ox

ratios in (a) and (b). The mean (square), 50th (horizontal line inside the box), 25th and 75th

percentiles (lower and upper box), and 10th and 90th percentiles (lower and upper whiskers) of the

box chart are marked in (c). The concentration of ALWC was simulated using the ISORROPIA-II model.

624

625

626

627

628
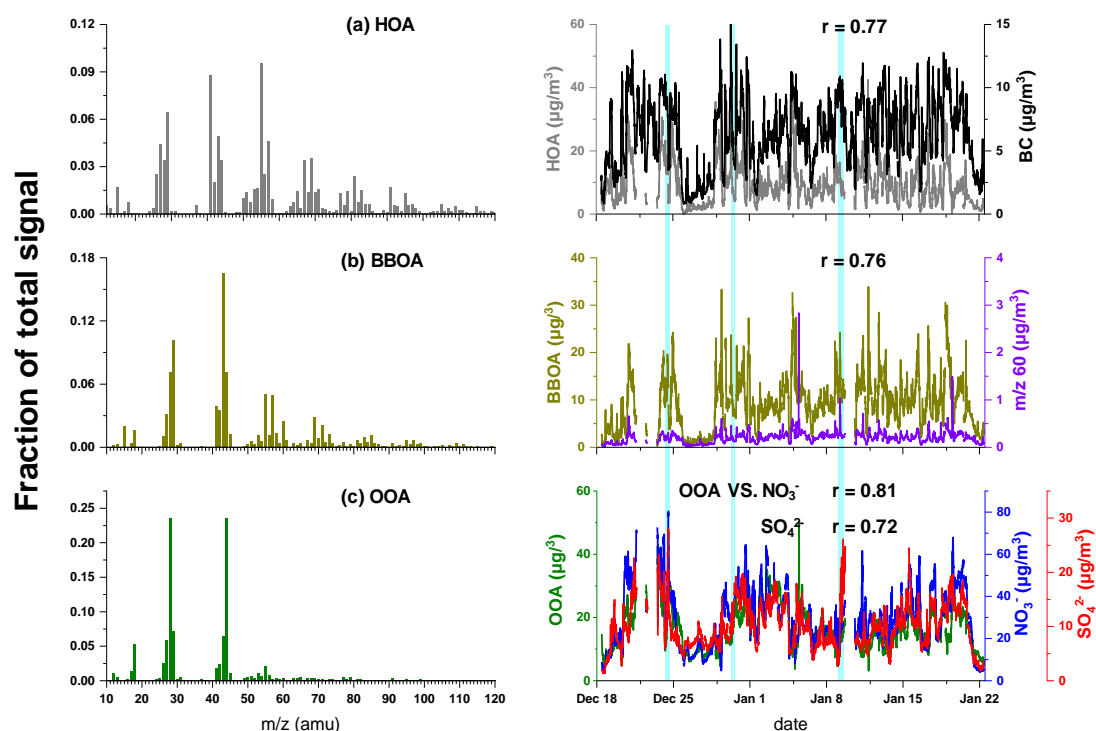
Fig. 5 Mass spectrum of (a) HOA, (b) BBOA, and (c) OOA resolved by PMF. The time series of
each OA source and corresponding tracers are depicted in the right panel. The light blue shaded
areas represent the intervals of foggy periods.

632

633

634
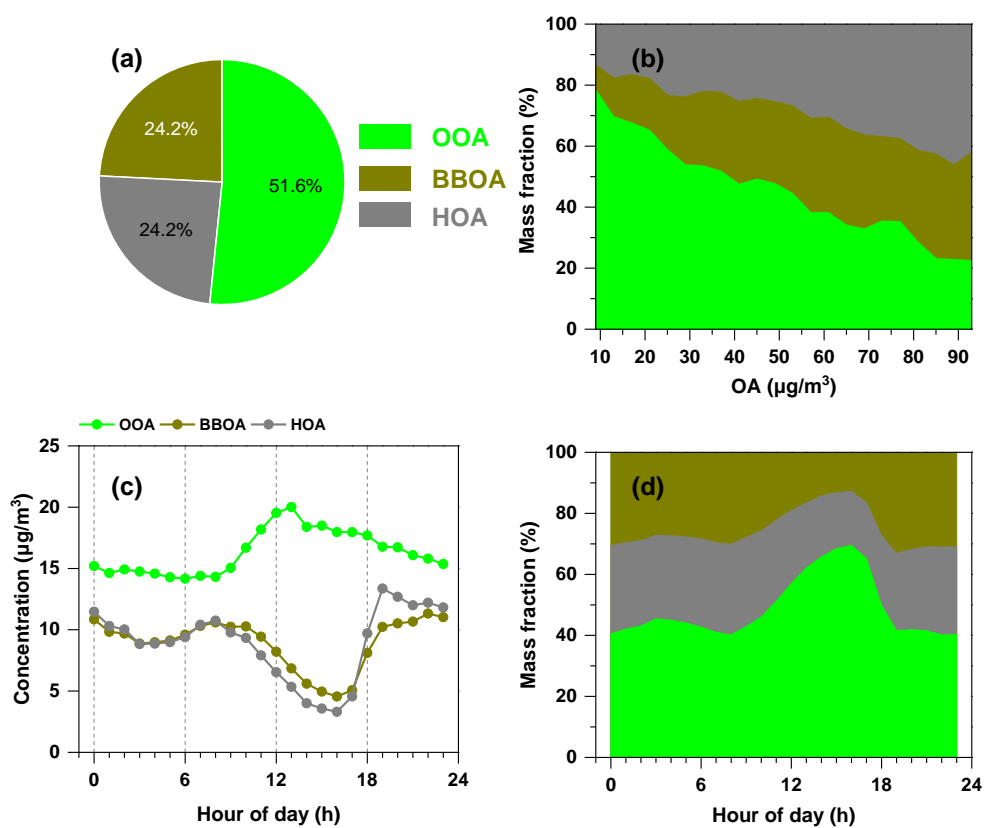
635 Fig. 6 Average mass fraction of different OOA, BBOA, and HOA (a) in OA and (b) as a function of

636 OA mass concentration. The diurnal variation of different OA factors compositions and their mass

637 contributions are shown in (c) and (d).

638

639

640

641
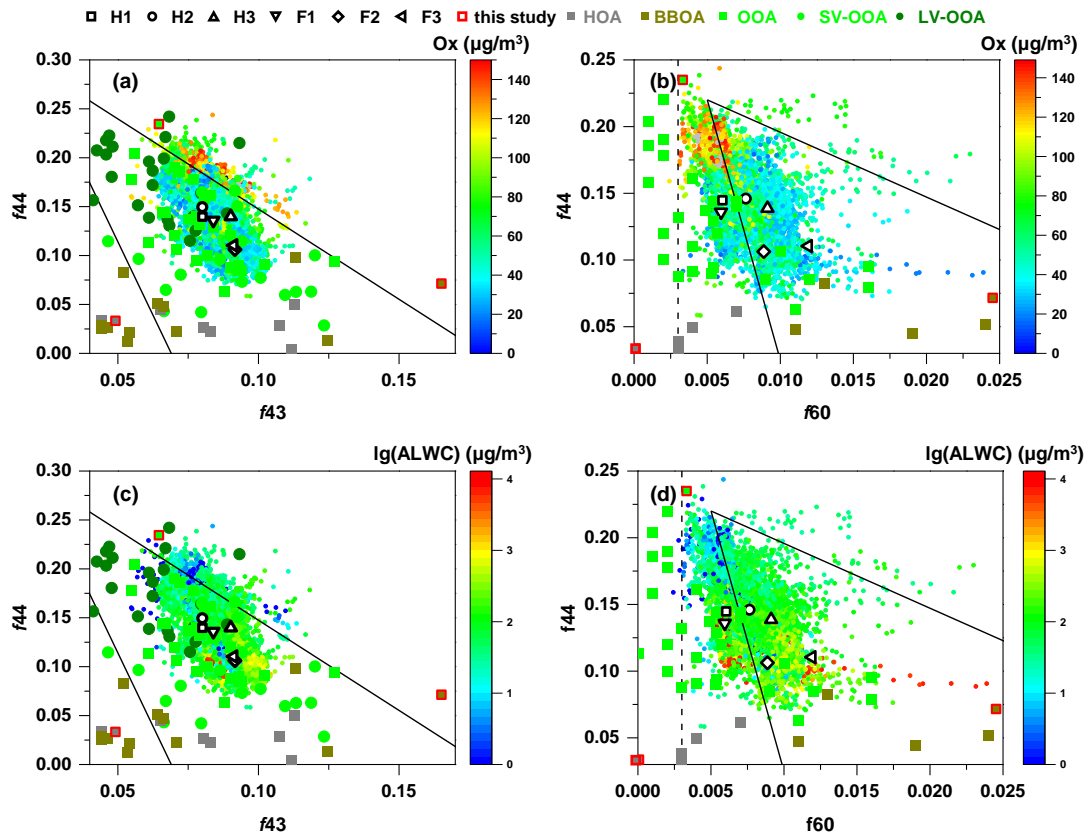
Fig. 7 Triangle plots of (a), (c) $f44$ (ratio of m/z 44 to total signal in the component mass spectrum)

vs. $f43$ (ratio of m/z 43 to total signal in the component mass spectrum), and (b), (d) $f44$ vs. $f60$

(ratio of m/z 60 to total signal in the component mass spectrum) during the whole campaign. The

colour scale in (a) and (b) represents Ox concentration, and that in (c) and (d) represents lg(ALWC).

The solid lines in (a) and (c) are derived from the results reported by Ng et al. (2010). The dashed

line representing the background value of secondary aged OA and the solid guidelines in (b) and (d)

are derived from Cubison et al. (2011). The $f44$ vs. $f43$ and $f44$ vs. $f60$ for different OA sources

reported in previous studies are also shown (Kim et al., 2019; Ng et al., 2011; Wang et al., 2016; Zhao

et al., 2019; Paglione et al., 2020).

651

652

653

654
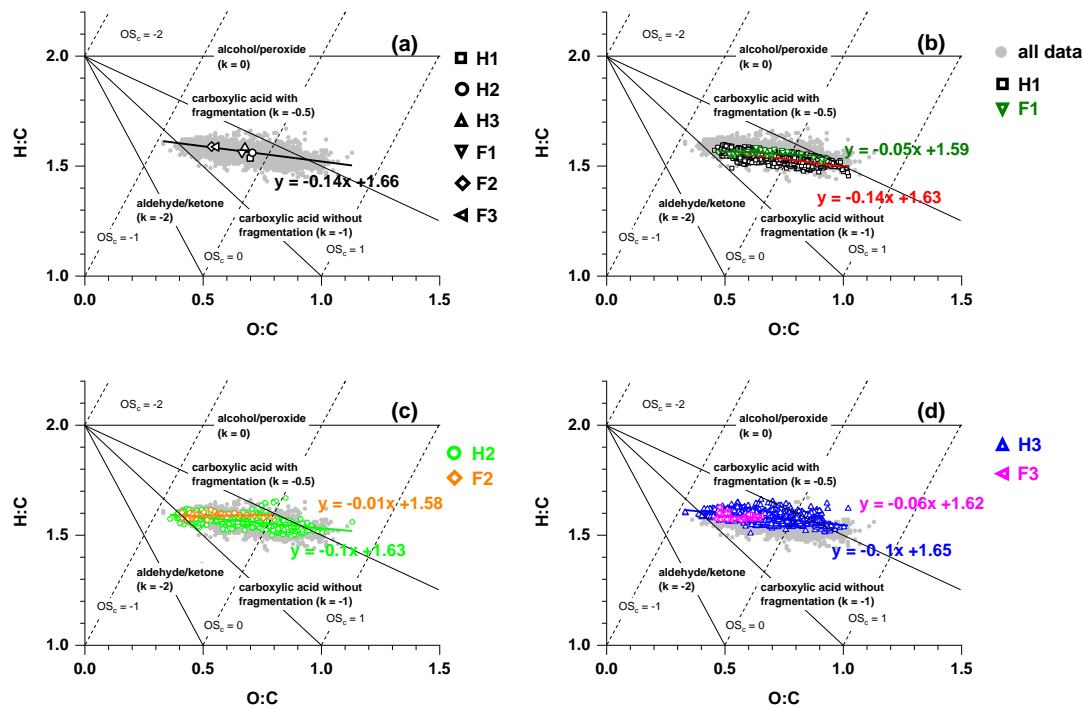
Fig. 8 The Van Krevelen-$\overline{OS_c}$ diagram with data during (a) the whole campaign, (b) H1 and F1, (c) H2 and F2, and (d) H3 and F3. The triangle lines with different slopes show distinct formation processes (Heald et al., 2010).

658

659

660

661

662
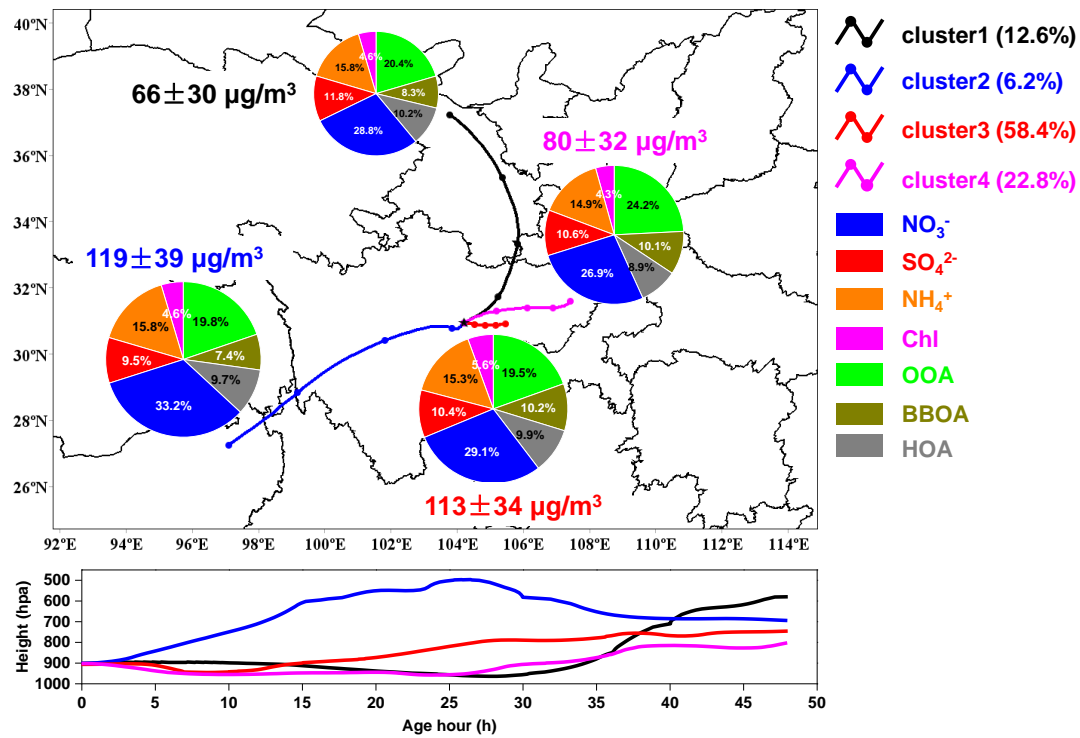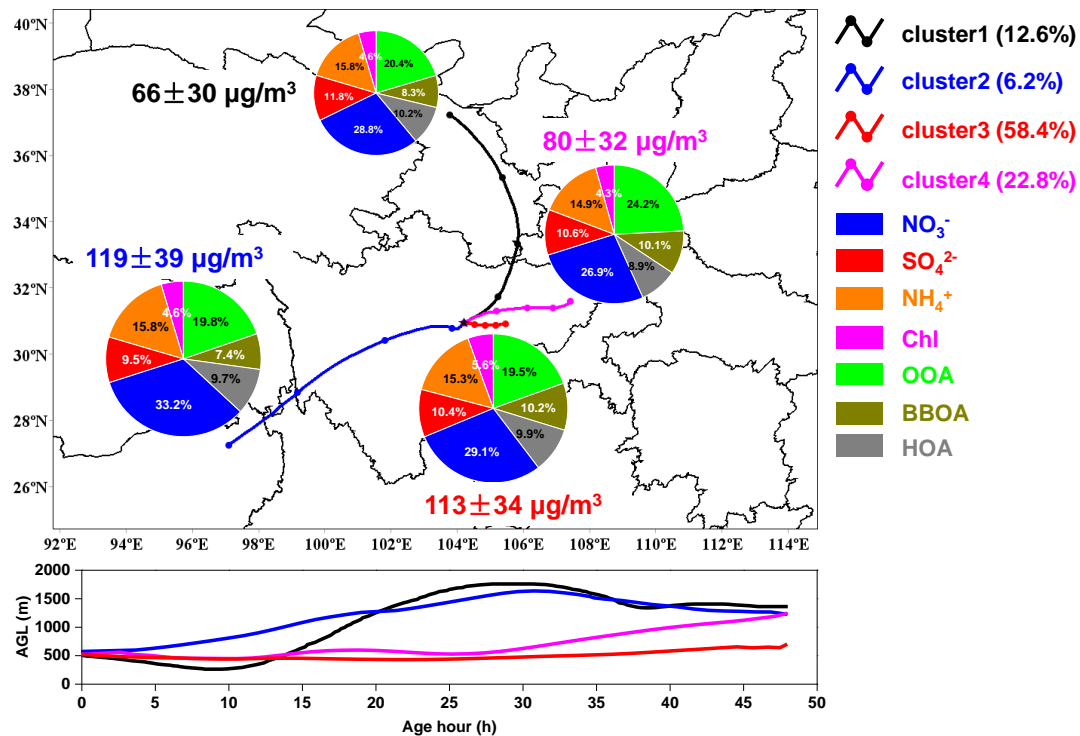
Fig. 9 Simulation results of 48 h backward air parcels cluster-mean trajectories during the campaign. The lines in black, blue, red, and purple represent the mean trajectories of cluster 1 to cluster 4, respectively. The pie charts show the average mass contribution of different chemical compositions

666   to PM$_{2.5}$ for each cluster. The lower panel shows the height profile (above ground level, AGL) for

667   different air parcels clusters along their transport paths.

668

669

670
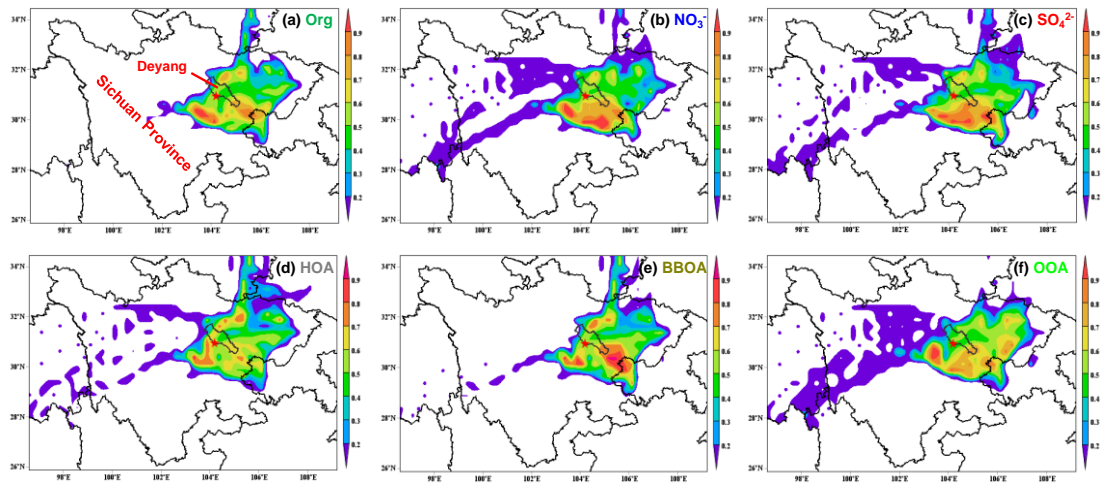
671

672 Fig. 10 Simulation results of PSCF for (a) organics, (b) nitrate, (c) sulphate, (d) HOA, (e) BBOA,

673 and (f) OOA during the whole campaign. The 50th percentile of the concentrations for each

674 composition (organics: 39.5 μg/m³, nitrate: 27.8 μg/m³, sulphate: 9.5 μg/m³, HOA: 7.6 μg/m³,

675 BBOA: 8.7 μg/m³, OOA: 15.2 μg/m³) were used as thresholds in the PSCF analysis. The areas of

676 Deyang and Sichuan Province are marked in (a).

677

678

679
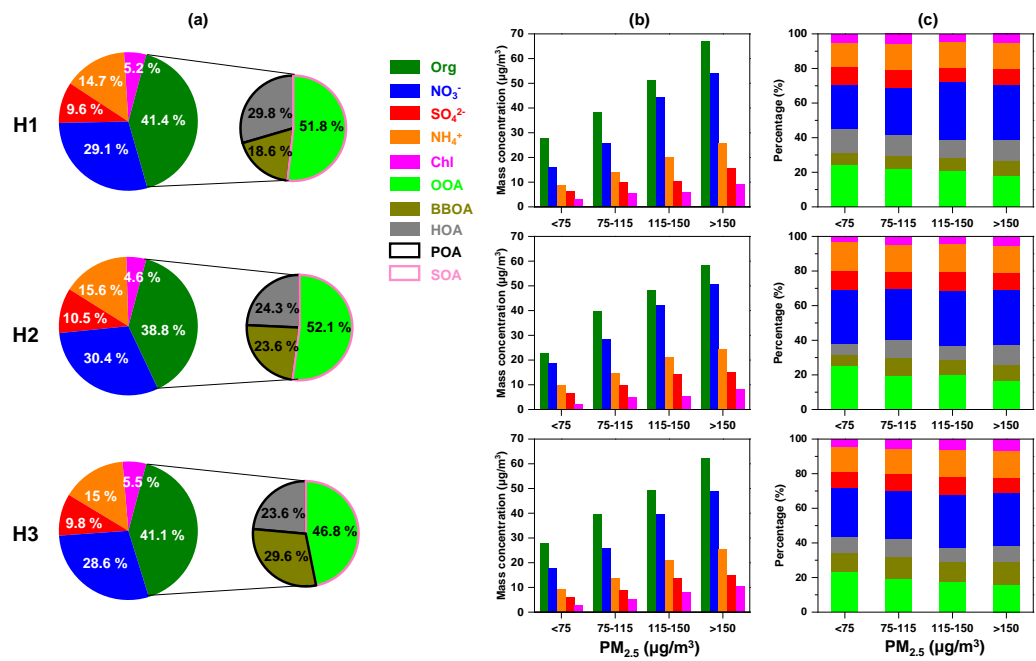
682 Fig. 11 (a) Average mass fractions of different chemical compositions in PM$_{2.5}$, (b) mass

683 concentration, and (c) relative contribution of inorganic/organic species as a function of PM$_{2.5}$

684 concentration during each haze episode. The right panel in (a) depicts the contribution of OOA,

685 BBOA, and HOA to OA.

686

687

688

689
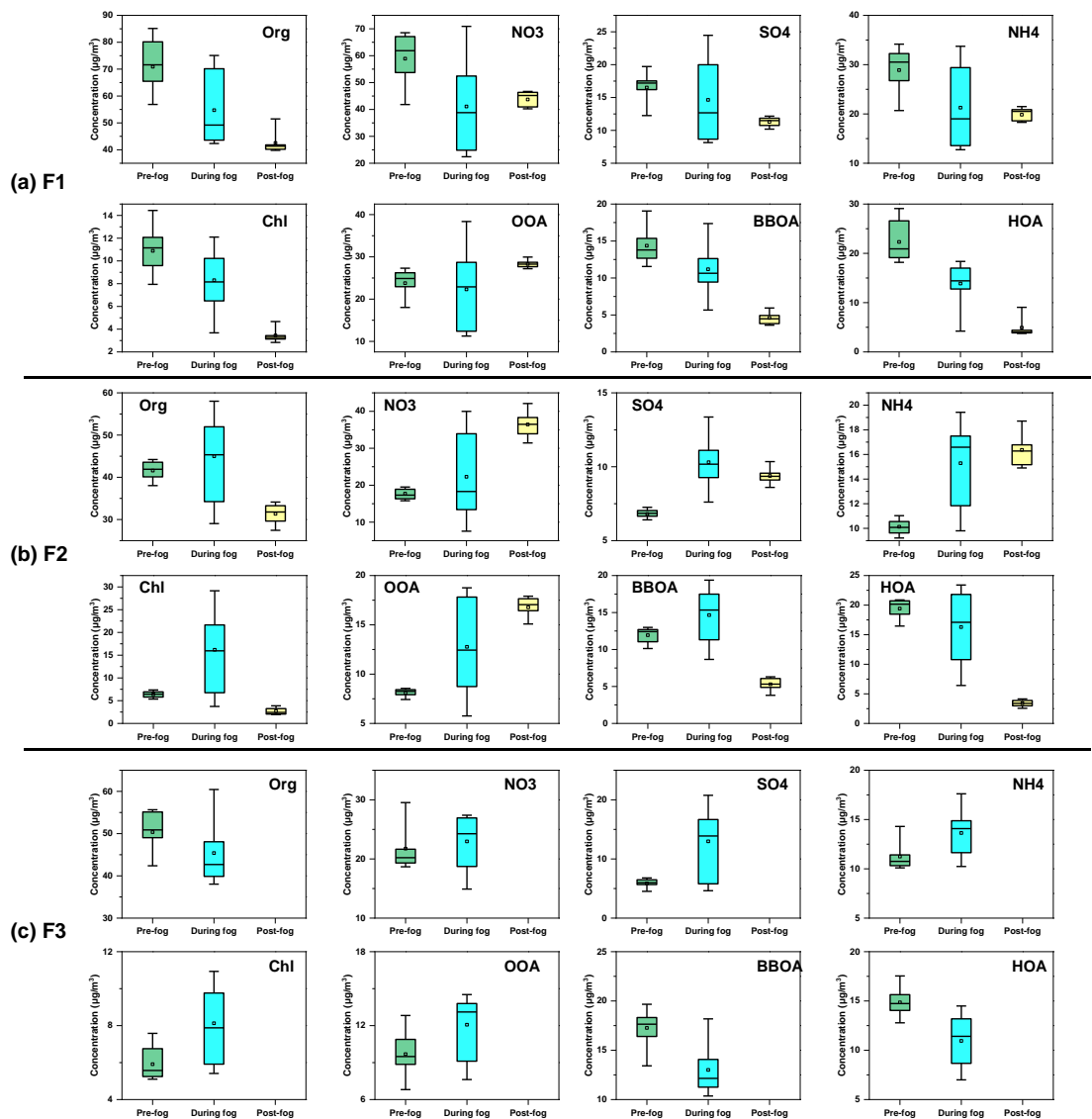
Fig. 12 Variation of organics, nitrate, sulphate, ammonium, chloride, OOA, BBOA, and HOA

concentration during the evolution of (a) F1, (b) F2, and (c) F3.

692

693

References

Aiken, A. C., Salcedo, D., Cubison, M. J., Huffman, J. A., DeCarlo, P. F., Ulbrich, I. M., Docherty, K. S., Sueper, D., Kimmel, J. R., Worsnop, D. R., Trimborn, A., Northway, M., Stone, E. A., Schauer, J. J., Volkamer, R. M., Fortner, E., de Foy, B., Wang, J., Laskin, A., Shutthanandan, V., Zheng, J., Zhang, R., Gaffney, J., Marley, N. A., Paredes-Miranda, G., Arnott, W. P., Molina, L. T., Sosa, G., and Jimenez, J. L.: Mexico City aerosol analysis during MILAGRO using high resolution aerosol mass spectrometry at the urban supersite (T0) – Part 1: Fine particle composition and organic source apportionment, Atmos. Chem. Phys., 6633-6653, 2009.

Alfarra, M. R., Prevot, A. S. H., Szidat, S., Sandradewi, J., Weimer, S., Lanz, V. A., Schreiber, D., Mohr, M., and Baltensperger, U.: Identification of the Mass Spectral Signature of Organic Aerosols from Wood Burning Emissions, Environ. Sci. Technol., 41, 5770-5777, https://doi.org/10.1021/es062289b, 2007.

Bao, Z., Chen, L., Li, K., Han, L., Wu, X., Gao, X., Azzi, M., and Cen, K.: Meteorological and chemical impacts on PM2.5 during a haze episode in a heavily polluted basin city of eastern China, Environ. Pollut., 250, 520-529, https://doi.org/10.1016/j.envpol.2019.04.045, 2019.

Boyd, C. M., Nah, T., Xu, L., Berkemeier, T., and Ng, N. L.: Secondary Organic Aerosol (SOA) from Nitrate Radical Oxidation of Monoterpenes: Effects of Temperature, Dilution, and Humidity on Aerosol Formation, Mixing, and Evaporation, Environ. Sci. Technol., 51, 7831-7841, https://doi.org/10.1021/acs.est.7b01460, 2017.

Canagaratna, M. R., Jimenez, J. L., Kroll, J. H., Chen, Q., Kessler, S. H., Massoli, P., Hildebrandt Ruiz, L., Fortner, E., Williams, L. R., Wilson, K. R., Surratt, J. D., Donahue, N. M., Jayne, J. T., and Worsnop, D. R.: Elemental ratio measurements of organic compounds using aerosol mass spectrometry: characterization, improved calibration, and implications, Atmos. Chem. Phys., 15, 253-272, https://doi.org/10.5194/acp-15-253-2015, 2015.

Chakraborty, A., Bhattu, D., Gupta, T., Tripathi, S. N., and Canagaratna, M. R.: Real-time measurements of ambient aerosols in a polluted Indian city: Sources, characteristics, and processing of organic aerosols during foggy and nonfoggy periods, J. Geophys. Res.-Atmos., 120, 9006-9019, https://doi.org/10.1002/2015JD023419, 2015.

Chakraborty, A., Gupta, T., and Tripathi, S. N.: Combined effects of organic aerosol loading and fog processing on organic aerosols oxidation, composition, and evolution, Sci. Total Environ., 573, 690-698, https://doi.org/10.1016/j.scitotenv.2016.08.156, 2016.

Chen, Q., Fu, T., Hu, J., Ying, Q., and Zhang, L.: Modelling secondary organic aerosols in China, Natl. Sci. Rev., 4, 806-809, 2017.

Chen, Q., Heald, C. L., Jimenez, J. L., Canagaratna, M. R., Zhang, Q., He, L. Y., Huang, X. F., Campuzano Jost, P., Palm, B. B., Poulain, L., Kuwata, M., Martin, S. T., Abbatt, J. P. D., Lee, A. K. Y., and Liggio, J.: Elemental composition of organic aerosol: The gap between ambient and laboratory measurements, Geophys. Res. Lett., 42, 4182-4189, https://doi.org/10.1002/2015GL063693, 2015.

Clark, C. H., Kacarab, M., Nakao, S., Asa-Awuku, A., Sato, K., and Cocker, D. R.: Temperature Effects on Secondary Organic Aerosol (SOA) from the Dark Ozonolysis and Photo-Oxidation of Isoprene, Environ. Sci. Technol., 50, 5564-5571, https://doi.org/10.1021/acs.est.5b05524, 2016.

Collett, J. L., Herckes, P., Youngster, S., and Lee, T.: Processing of atmospheric organic matter by California radiation fogs, Atmos. Res., 87, 232-241, https://doi.org/10.1016/j.atmosres.2007.11.005, 2008.

Cubison, M. J., Ortega, A. M., Hayes, P. L., Farmer, D. K., Day, D., Lechner, M. J., Brune, W. H., Apel, E., Diskin, G. S., Fisher, J. A., Fuelberg, H. E., Hecobian, A., Knapp, D. J., Mikoviny, T., Riemer, D., Sachse, G. W., Sessions, W., Weber, R. J., Weinheimer, A. J., Wisthaler, A., and Jimenez, J. L.: Effects of aging on organic aerosol from open biomass burning smoke in aircraft and laboratory studies, Atmos. Chem. Phys., 11, 12049-12064, https://doi.org/10.5194/acp-11-12049-2011, 2011.

Dai, Q., Schulze, B. C., Bi, X., Bui, A. A. T., Guo, F., Wallace, H. W., Sanchez, N. P., Flynn, J. H., Lefer, B. L., Feng, Y., and Griffin, R. J.: Seasonal differences in formation processes of oxidized organic aerosol near Houston, TX, Atmos. Chem. Phys., 19, 9641-9661, https://doi.org/10.5194/acp-19-9641-2019, 2019.

Ding, A., Huang, X., Nie, W., Chi, X., Xu, Z., Zheng, L., Xu, Z., Xie, Y., Qi, X., Shen, Y., Sun, P., Wang, J., Wang, L., Sun, J., Yang, X., Qin, W., Zhang, X., Cheng, W., Liu, W., Pan, L., and Fu, C.: Significant reduction of PM2.5 in eastern China due to regional-scale emission control: evidence from SORPES in 2011-2018, Atmos. Chem. Phys., 19, 11791-11801, https://doi.org/10.5194/acp-19-11791-2019, 2019.

Docherty, K. S., Corse, E. W., Jaoui, M., Offenberg, J. H., Kleindienst, T. E., Krug, J. D., Riedel, T. P.,

and Lewandowski, M.: Trends in the oxidation and relative volatility of chamber-generated secondary organic aerosol, Aerosol Sci. Tech., 52, 992-1004, https://doi.org/10.1080/02786826.2018.1500014, 2018.

Docherty, K. S., Stone, E. A., Ulbrich, I. M., DeCarlo, P. F., Snyder, D. C., Schauer, J. J., Peltier, R. E., Weber, R. J., Murphy, S. M., Seinfeld, J. H., Grover, B. D., Eatough, D. J., and Jimenez, J. L.: Apportionment of Primary and Secondary Organic Aerosols in Southern California during the 2005 Study of Organic Aerosols in Riverside (SOAR-1), Environ. Sci. Technol., 42, 7655-7662, https://doi.org/10.1021/es8008166, 2008.

Donahue, N. M., Robinson, A. L., Stanier, C. O., and Pandis, S. N.: Coupled Partitioning, Dilution, and Chemical Aging of Semivolatile Organics, Environ. Sci. Technol., 40, 2635-2643, https://doi.org/10.1021/es052297c, 2006.

Draxler, R. R., and Hess, G. D.: An overview of the HYSPLIT_4 modeling system for trajectories, dispersion, and deposition, Aust. Meteor. Mag., 47, 295-308, 1998.

Duan, J., Huang, R., Gu, Y., Lin, C., Zhong, H., Wang, Y., Yuan, W., Ni, H., Yang, L., Chen, Y., Worsnop, D. R., and O'Dowd, C.: The formation and evolution of secondary organic aerosol during summer in Xi'an: Aqueous phase processing in fog-rain days, Sci. Total Environ., 756, 144077, https://doi.org/10.1016/j.scitotenv.2020.144077, 2021.

Fröhlich, R., Cubison, M. J., Slowik, J. G., Bukowiecki, N., Prévôt, A. S. H., Baltensperger, U., Schneider, J., Kimmel, J. R., Gonin, M., Rohner, U., Worsnop, D. R., and Jayne, J. T.: The ToF-ACSM: a portable aerosol chemical speciation monitor with TOFMS detection, Atmos. Meas. Tech., 6, 3225-3241, https://doi.org/10.5194/amt-6-3225-2013, 2013.

Fu, X., Wang, S., Xing, J., Zhang, X., Wang, T., and Hao, J.: Increasing Ammonia Concentrations Reduce the Effectiveness of Particle Pollution Control Achieved via SO2 and NOx Emissions Reduction in East China, Environ. Sci. Technol. Lett., 4, 221-227, https://doi.org/10.1021/acs.estlett.7b00143, 2017.

Fu, X., Wang, T., Gao, J., Wang, P., Liu, Y., Wang, S., Zhao, B., and Xue, L.: Persistent Heavy Winter Nitrate Pollution Driven by Increased Photochemical Oxidants in Northern China, Environ. Sci. Technol., 54, 3881-3889, https://doi.org/10.1021/acs.est.9b07248, 2020.

Ge, D., Nie, W., Sun, P., Liu, Y., Wang, T., Wang, J., Wang, J., Wang, L., Zhu, C., Wang, R., Liu, T., Chi, X., and Ding, A.: Characterization of particulate organic nitrates in the Yangtze River Delta, East

China, using the time-of-flight aerosol chemical speciation monitor, Atmos. Environ., 272, 118927, https://doi.org/10.1016/j.atmosenv.2021.118927, 2022.

Ge, X., Li, L., Chen, Y., Chen, H., Wu, D., Wang, J., Xie, X., Ge, S., Ye, Z., Xu, J., and Chen, M.: Aerosol characteristics and sources in Yangzhou, China resolved by offline aerosol mass spectrometry and other techniques, Environ. Pollut., 225, 74-85, https://doi.org/10.1016/j.envpol.2017.03.044, 2017.

Gilardoni, S., Massoli, P., Paglione, M., Giulianelli, L., Carbone, C., Rinaldi, M., Decesari, S., Sandrini, S., Costabile, F., Gobbi, G. P., Pietrogrande, M. C., Visentin, M., Scotto, F., Fuzzi, S., and Facchini, M. C.: Direct observation of aqueous secondary organic aerosol from biomass-burning emissions, P. Natl. Acad. Sci. USA, 113, 10013-10018, https://doi.org/10.1073/pnas.1602212113, 2016.

Guo, J., Zhou, S., Cai, M., Zhao, J., Song, W., Zhao, W., Hu, W., Sun, Y., He, Y., Yang, C., Xu, X., Zhang, Z., Cheng, P., Fan, Q., Hang, J., Fan, S., Wang, X., and Wang, X.: Characterization of submicron particles by time-of-flight aerosol chemical speciation monitor (ToF-ACSM) during wintertime: aerosol composition, sources, and chemical processes in Guangzhou, China, Atmos. Chem. Phys., 20, 7595-7615, https://doi.org/10.5194/acp-20-7595-2020, 2020.

Guo, L., Guo, X., Fang, C., and Zhu, S.: Observation analysis on characteristics of formation, evolution and transition of a long-lasting severe fog and haze episode in North China, Sci. China Earth Sci., 58, 329-344, https://doi.org/10.1007/s11430-014-4924-2, 2015.

Guo, S., Hu, M., Zamora, M. L., Peng, J., Shang, D., Zheng, J., Du, Z., Wu, Z., Shao, M., Zeng, L., Molina, M. J., and Zhang, R.: Elucidating severe urban haze formation in China, P. Natl. Acad. Sci. USA, 111, 17373-17378, https://doi.org/10.1073/pnas.1419604111, 2014.

He, K., Zhao, Q., Ma, Y., Duan, F., Yang, F., Shi, Z., and Chen, G.: Spatial and seasonal variability of PM2.5 acidity at two Chinese megacities: insights into the formation of secondary inorganic aerosols, Atmos. Chem. Phys., 12, 1377-1395, https://doi.org/10.5194/acp-12-1377-2012, 2012.

Heald, C. L., Kroll, J. H., Jimenez, J. L., Docherty, K. S., DeCarlo, P. F., Aiken, A. C., Chen, Q., Martin, S. T., Farmer, D. K., and Artaxo, P.: A simplified description of the evolution of organic aerosol composition in the atmosphere, Geophys. Res. Lett., 37, https://doi.org/10.1029/2010GL042737, 2010.

Herndon, S. C., Onasch, T. B., Wood, E. C., Kroll, J. H., Canagaratna, M. R., Jayne, J. T., Zavala, M. A., Knighton, W. B., Mazzoleni, C., Dubey, M. K., Ulbrich, I. M., Jimenez, J. L., Seila, R., de Gouw,

J. A., de Foy, B., Fast, J., Molina, L. T., Kolb, C. E., and Worsnop, D. R.: Correlation of secondary organic aerosol with odd oxygen in Mexico City, Geophys. Res. Lett., 35, https://doi.org/10.1029/2008GL034058, 2008.

Hinks, M. L., Montoya-Aguilera, J., Ellison, L., Lin, P., Laskin, A., Laskin, J., Shiraiwa, M., Dabdub, D., and Nizkorodov, S. A.: Effect of relative humidity on the composition of secondary organic aerosol from the oxidation of toluene, Atmos. Chem. Phys., 18, 1643-1652, https://doi.org/10.5194/acp-18-1643-2018, 2018.

Huang, R., Zhang, Y., Bozzetti, C., Ho, K., Cao, J., Han, Y., Daellenbach, K. R., Slowik, J. G., Platt, S. M., Canonaco, F., Zotter, P., Wolf, R., Pieber, S. M., Bruns, E. A., Crippa, M., Ciarelli, G., Piazzalunga, A., Schwikowski, M., Abbaszade, G., Schnelle-Kreis, J., Zimmermann, R., An, Z., Szidat, S., Baltensperger, U., Haddad, I. E., and Prévôt, A. S. H.: High secondary aerosol contribution to particulate pollution during haze events in China, Nature, 514, 218-222, https://doi.org/10.1038/nature13774, 2014.

Huang, X., Zhang, J., Zhang, W., Tang, G., and Wang, Y.: Atmospheric ammonia and its effect on PM2.5 pollution in urban Chengdu, Sichuan Basin, China, Environ. Pollut., 291, 118195, https://doi.org/10.1016/j.envpol.2021.118195, 2021.

Ianniello, A., Spataro, F., Esposito, G., Allegrini, I., Hu, M., and Zhu, T.: Chemical characteristics of inorganic ammonium salts in PM2.5 in the atmosphere of Beijing (China), Atmos. Chem. Phys., 11, 10803-10822, https://doi.org/10.5194/acp-11-10803-2011, 2011.

Izhar, S., Gupta, T., and Panday, A. K.: Scavenging efficiency of water soluble inorganic and organic aerosols by fog droplets in the Indo Gangetic Plain, Atmos. Res., 235, 104767, https://doi.org/10.1016/j.atmosres.2019.104767, 2020.

Kim, H., Collier, S., Ge, X., Xu, J., Sun, Y., Jiang, W., Wang, Y., Herckes, P., and Zhang, Q.: Chemical processing of water-soluble species and formation of secondary organic aerosol in fogs, Atmos. Environ., 200, 158-166, https://doi.org/10.1016/j.atmosenv.2018.11.062, 2019.

Kong, L., Tan, Q., Feng, M., Qu, Y., An, J., Liu, X., Cheng, N., Deng, Y., Zhai, R., and Wang, Z.: Investigating the characteristics and source analyses of PM2.5 seasonal variations in Chengdu, Southwest China, Chemosphere, 243, 125267, https://doi.org/10.1016/j.chemosphere.2019.125267, 2020.

Kuang, Y., He, Y., Xu, W., Yuan, B., Zhang, G., Ma, Z., Wu, C., Wang, C., Wang, S., Zhang, S., Tao,

J., Ma, N., Su, H., Cheng, Y., Shao, M., and Sun, Y.: Photochemical Aqueous-Phase Reactions Induce Rapid Daytime Formation of Oxygenated Organic Aerosol on the North China Plain, Environ. Sci. Technol., 54, 3849-3860, https://doi.org/10.1021/acs.est.9b06836, 2020.

Lanz, V. A., Alfarra, M. R., Baltensperger, U., Buchmann, B., Hueglin, C., and Prévôt, A. S. H.: Source apportionment of submicron organic aerosols at an urban site by factor analytical modelling of aerosol mass spectra, Atmos. Chem. Phys., 7, 1503-1522, https://doi.org/10.5194/acp-7-1503-2007, 2007.

Li, H., Zhang, Q., Zheng, B., Chen, C., Wu, N., Guo, H., Zhang, Y., Zheng, Y., Li, X., and He, K.: Nitrate-driven urban haze pollution during summertime over the North China Plain, Atmos. Chem. Phys., 18, 5293-5306, https://doi.org/10.5194/acp-18-5293-2018, 2018.

Liu, M., Huang, X., Song, Y., Tang, J., Cao, J., Zhang, X., Zhang, Q., Wang, S., Xu, T., Kang, L., Cai, X., Zhang, H., Yang, F., Wang, H., Yu, J. Z., Lau, A. K. H., He, L., Huang, X., Duan, L., Ding, A., Xue, L., Gao, J., Liu, B., and Zhu, T.: Ammonia emission control in China would mitigate haze pollution and nitrogen deposition, but worsen acid rain, Proceedings of the National Academy of Sciences, 116, 7760-7765, https://doi.org/10.1073/pnas.1814880116, 2019.

Liu, M., Huang, X., Song, Y., Xu, T., Wang, S., Wu, Z., Hu, M., Zhang, L., Zhang, Q., Pan, Y., Liu, X., and Zhu, T.: Rapid SO2 emission reductions significantly increase tropospheric ammonia concentrations over the North China Plain, Atmos. Chem. Phys., 18, 17933-17943, https://doi.org/10.5194/acp-18-17933-2018, 2018.

Liu, P. S. K., Deng, R., Smith, K. A., Williams, L. R., Jayne, J. T., Canagaratna, M. R., Moore, K., Onasch, T. B., Worsnop, D. R., and Deshler, T.: Transmission Efficiency of an Aerodynamic Focusing Lens System: Comparison of Model Calculations and Laboratory Measurements for the Aerodyne Aerosol Mass Spectrometer, Aerosol Sci. Tech., 41, 721-733, https://doi.org/10.1080/02786820701422278, 2007.

Liu, P., Ye, C., Xue, C., Zhang, C., Mu, Y., and Sun, X.: Formation mechanisms of atmospheric nitrate and sulfate during the winter haze pollution periods in Beijing: gas-phase, heterogeneous and aqueous-phase chemistry, Atmos. Chem. Phys., 20, 4153-4165, https://doi.org/10.5194/acp-20-4153-2020, 2020.

Liu, T., Huang, D. D., Li, Z., Liu, Q., Chan, M., and Chan, C. K.: Comparison of secondary organic aerosol formation from toluene on initially wet and dry ammonium sulfate particles at moderate relative humidity, Atmos. Chem. Phys., 18, 5677-5689, https://doi.org/10.5194/acp-18-5677-2018,

2018.

Mandariya, A. K., Gupta, T., and Tripathi, S. N.: Effect of aqueous-phase processing on the formation and evolution of organic aerosol (OA) under different stages of fog life cycles, Atmos. Environ., 206, 60-71, https://doi.org/10.1016/j.atmosenv.2019.02.047, 2019.

Matthew, B. M., Middlebrook, A. M., and Onasch, T. B.: Collection Efficiencies in an Aerodyne Aerosol Mass Spectrometer as a Function of Particle Phase for Laboratory Generated Aerosols, Aerosol Sci. Tech., 42, 884-898, https://doi.org/10.1080/02786820802356797, 2008.

Middlebrook, A. M., Bahreini, R., Jimenez, J. L., and Canagaratna, M. R.: Evaluation of Composition-Dependent Collection Efficiencies for the Aerodyne Aerosol Mass Spectrometer using Field Data, Aerosol Sci. Tech., 46, 258-271, https://doi.org/10.1080/02786826.2011.620041, 2012.

Mohr, C., DeCarlo, P. F., Heringa, M. F., Chirico, R., Slowik, J. G., Richter, R., Reche, C., Alastuey, A., Querol, X., Seco, R., Peñuelas, J., Jiménez, J. L., Crippa, M., Zimmermann, R., Baltensperger, U., and Prévôt, A. S. H.: Identification and quantification of organic aerosol from cooking and other sources in Barcelona using aerosol mass spectrometer data, Atmos. Chem. Phys., 12, 1649-1665, https://doi.org/10.5194/acp-12-1649-2012, 2012.

Ng, N. L., Canagaratna, M. R., Jimenez, J. L., Chhabra, P. S., Seinfeld, J. H., and Worsnop, D. R.: Changes in organic aerosol composition with aging inferred from aerosol mass spectra, Atmos. Chem. Phys., 11, 6465-6474, https://doi.org/10.5194/acp-11-6465-2011, 2011.

Ng, N. L., Canagaratna, M. R., Zhang, Q., Jimenez, J. L., Tian, J., Ulbrich, I. M., Kroll, J. H., Docherty, K. S., Chhabra, P. S., Bahreini, R., Murphy, S. M., Seinfeld, J. H., Hildebrandt, L., Donahue, N. M., DeCarlo, P. F., Lanz, V. A., Prévôt, A. S. H., Dinar, E., Rudich, Y., and Worsnop, D. R.: Organic aerosol components observed in Northern Hemispheric datasets from Aerosol Mass Spectrometry, Atmos. Chem. Phys., 10, 4625-4641, https://doi.org/10.5194/acp-10-4625-2010, 2010.

Ng, N. L., Herndon, S. C., Trimborn, A., Canagaratna, M. R., Croteau, P. L., Onasch, T. B., Sueper, D., Worsnop, D. R., Zhang, Q., Sun, Y. L., and Jayne, J. T.: An Aerosol Chemical Speciation Monitor (ACSM) for Routine Monitoring of the Composition and Mass Concentrations of Ambient Aerosol, Aerosol Sci. Tech., 45, 780-794, https://doi.org/10.1080/02786826.2011.560211, 2011.

Paatero, P., and Tapper, U.: Positive matrix factorization: A non-negative factor model with optimal utilization of error estimates of data values, Environmetrics, 5, 111-126, 1994.

Paglione, M., Gilardoni, S., Rinaldi, M., Decesari, S., Zanca, N., Sandrini, S., Giulianelli, L., Bacco, D.,

Ferrari, S., Poluzzi, V., Scotto, F., Trentini, A., Poulain, L., Herrmann, H., Wiedensohler, A., Canonaco, F., Prévôt, A. S. H., Massoli, P., Carbone, C., Facchini, M. C., and Fuzzi, S.: The impact of biomass burning and aqueous-phase processing on air quality: a multi-year source apportionment study in the Po Valley, Italy, Atmos. Chem. Phys., 20, 1233-1254, https://doi.org/10.5194/acp-20-1233-2020, 2020.

Pathak, R. K., Wu, W. S., and Wang, T.: Summertime PM2.5 ionic species in four major cities of China: nitrate formation in an ammonia-deficient atmosphere, Atmos. Chem. Phys., 9, 1711-1722, https://doi.org/10.5194/acp-9-1711-2009, 2009.

Peng, J., Hu, M., Shang, D., Wu, Z., Du, Z., Tan, T., Wang, Y., Zhang, F., and Zhang, R.: Explosive Secondary Aerosol Formation during Severe Haze in the North China Plain, Environ. Sci. Technol., 55, 2189-2207, https://doi.org/10.1021/acs.est.0c07204, 2021.

Polissar, A. V., Hopke, P. K., and Harris, J. M.: Source Regions for Atmospheric Aerosol Measured at Barrow, Alaska, Environ. Sci. Technol., 35, 4214-4226, https://doi.org/10.1021/es0107529, 2001.

Rollins, A. W., Browne, E. C., Min, K., Pusede, S. E., Wooldridge, P. J., Gentner, D. R., Goldstein, A. H., Liu, S., Day, D. A., and Russell, L. M.: Evidence for NO x control over nighttime SOA formation, Science, 337, 1210-1212, 2012.

Song, M., Liu, X., Tan, Q., Feng, M., Qu, Y., An, J., and Zhang, Y.: Characteristics and formation mechanism of persistent extreme haze pollution events in Chengdu, southwestern China, Environ. Pollut., 251, 1-12, https://doi.org/10.1016/j.envpol.2019.04.081, 2019.

Sun, Y. L., Zhang, Q., Anastasio, C., and Sun, J.: Insights into secondary organic aerosol formed via aqueous-phase reactions of phenolic compounds based on high resolution mass spectrometry, Atmos. Chem. Phys., 10, 4809-4822, https://doi.org/10.5194/acp-10-4809-2010, 2010.

Sun, Y. L., Zhang, Q., Schwab, J. J., Demerjian, K. L., Chen, W. N., Bae, M. S., Hung, H. M., Hogrefe, O., Frank, B., Rattigan, O. V., and Lin, Y. C.: Characterization of the sources and processes of organic and inorganic aerosols in New York city with a high-resolution time-of-flight aerosol mass apectrometer, Atmos. Chem. Phys., 11, 1581-1602, https://doi.org/10.5194/acp-11-1581-2011, 2011.

Sun, Y., Chen, C., Zhang, Y., Xu, W., Zhou, L., Cheng, X., Zheng, H., Ji, D., Li, J., Tang, X., Fu, P., and Wang, Z.: Rapid formation and evolution of an extreme haze episode in Northern China during winter 2015, Sci. Rep.-UK, 6, https://doi.org/10.1038/srep27151, 2016.

Sun, Y., He, Y., Kuang, Y., Xu, W., Song, S., Ma, N., Tao, J., Cheng, P., Wu, C., Su, H., Cheng, Y., Xie,

C., Chen, C., Lei, L., Qiu, Y., Fu, P., Croteau, P., and Worsnop, D. R.: Chemical Differences Between PM1 and PM2.5 in Highly Polluted Environment and Implications in Air Pollution Studies, Geophys. Res. Lett., 47, https://doi.org/10.1029/2019GL086288, 2020.

Sun, Y., Jiang, Q., Xu, Y., Ma, Y., Zhang, Y., Liu, X., Li, W., Wang, F., Li, J., Wang, P., and Li, Z.: Aerosol characterization over the North China Plain: Haze life cycle and biomass burning impacts in summer, J. Geophys. Res.-Atmos., 121, 2508-2521, https://doi.org/10.1002/2015JD024261, 2016.

Tan, Z., Lu, K., Jiang, M., Su, R., Wang, H., Lou, S., Fu, Q., Zhai, C., Tan, Q., Yue, D., Chen, D., Wang, Z., Xie, S., Zeng, L., and Zhang, Y.: Daytime atmospheric oxidation capacity in four Chinese megacities during the photochemically polluted season: a case study based on box model simulation, Atmos. Chem. Phys., 19, 3493-3513, https://doi.org/10.5194/acp-19-3493-2019, 2019.

Tao, J., Zhang, L., Cao, J., and Zhang, R.: A review of current knowledge concerning PM2. 5 chemical composition, aerosol optical properties and their relationships across China, Atmos. Chem. Phys., 17, 9485-9518, https://doi.org/10.5194/acp-17-9485-2017, 2017.

Tian, M., Liu, Y., Yang, F., Zhang, L., Peng, C., Chen, Y., Shi, G., Wang, H., Luo, B., Jiang, C., Li, B., Takeda, N., and Koizumi, K.: Increasing importance of nitrate formation for heavy aerosol pollution in two megacities in Sichuan Basin, southwest China, Environ. Pollut., 250, 898-905, https://doi.org/10.1016/j.envpol.2019.04.098, 2019.

Ulbrich, I. M., Canagaratna, M. R., Zhang, Q., Worsnop, D. R., and Jimenez, J. L.: Interpretation of organic components from Positive Matrix Factorization of aerosol mass spectrometric data, Atmos. Chem. Phys., 9, 2891-2918, 2009.

Wang, G., Zhang, R., Gomez, M. E., Yang, L., Levy Zamora, M., Hu, M., Lin, Y., Peng, J., Guo, S., Meng, J., Li, J., Cheng, C., Hu, T., Ren, Y., Wang, Y., Gao, J., Cao, J., An, Z., Zhou, W., Li, G., Wang, J., Tian, P., Marrero-Ortiz, W., Secrest, J., Du, Z., Zheng, J., Shang, D., Zeng, L., Shao, M., Wang, W., Huang, Y., Wang, Y., Zhu, Y., Li, Y., Hu, J., Pan, B., Cai, L., Cheng, Y., Ji, Y., Zhang, F., Rosenfeld, D., Liss, P. S., Duce, R. A., Kolb, C. E., and Molina, M. J.: Persistent sulfate formation from London Fog to Chinese haze, P. Natl. Acad. Sci. USA, 113, 13630-13635, https://doi.org/10.1073/pnas.1616540113, 2016.

Wang, H., Tian, M., Chen, Y., Shi, G., Liu, Y., Yang, F., Zhang, L., Deng, L., Yu, J., Peng, C., and Cao, X.: Seasonal characteristics, formation mechanisms and source origins of PM2.5 in two megacities in Sichuan Basin, China, Atmos. Chem. Phys., 18, 865-881, https://doi.org/10.5194/acp-18-865-2018,

2018.

Wang, J., Ge, X., Chen, Y., Shen, Y., Zhang, Q., Sun, Y., Xu, J., Ge, S., Yu, H., and Chen, M.: Highly time-resolved urban aerosol characteristics during springtime inYangtze River Delta, China: insights from soot particle aerosol massspectrometry, Atmos. Chem. Phys., 16, 9109-9127, https://doi.org/10.5194/acp-16-9109-2016, 2016.

Wang, J., Li, J., Ye, J., Zhao, J., Wu, Y., Hu, J., Liu, D., Nie, D., Shen, F., Huang, X., Huang, D. D., Ji, D., Sun, X., Xu, W., Guo, J., Song, S., Qin, Y., Liu, P., Turner, J. R., Lee, H. C., Hwang, S., Liao, H., Martin, S. T., Zhang, Q., Chen, M., Sun, Y., Ge, X., and Jacob, D. J.: Fast sulfate formation from oxidation of SO2 by NO2 and HONO observed in Beijing haze, Nat. Commun., 11, https://doi.org/10.1038/s41467-020-16683-x, 2020.

Wang, J., Ye, J., Zhang, Q., Zhao, J., Wu, Y., Li, J., Liu, D., Li, W., Zhang, Y., Wu, C., Xie, C., Qin, Y., Lei, Y., Huang, X., Guo, J., Liu, P., Fu, P., Li, Y., Lee, H. C., Choi, H., Zhang, J., Liao, H., Chen, M., Sun, Y., Ge, X., Martin, S. T., and Jacob, D. J.: Aqueous production of secondary organic aerosol from fossil-fuel emissions in winter Beijing haze, P. Natl. Acad. Sci. USA, 118, https://doi.org/10.1073/pnas.2022179118, 2021.

Wang, Y., Yao, L., Wang, L., Liu, Z., Ji, D., Tang, G., Zhang, J., Sun, Y., Hu, B., and Xin, J.: Mechanism for the formation of the January 2013 heavy haze pollution episode over central and eastern China, Sci. China Earth Sci., 57, 14-25, https://doi.org/10.1007/s11430-013-4773-4, 2014.

Weimer, S., Alfarra, M. R., Schreiber, D., Mohr, M., Prévôt, A. S. H., and Baltensperger, U.: Organic aerosol mass spectral signatures from wood-burning emissions: Influence of burning conditions and wood type, J. Geophys. Res., 113, https://doi.org/10.1029/2007JD009309, 2008.

Wen, L., Xue, L., Wang, X., Xu, C., Chen, T., Yang, L., Wang, T., Zhang, Q., and Wang, W.: Summertime fine particulate nitrate pollution in the North China Plain: increasing trends, formation mechanisms and implications for control policy, Atmos. Chem. Phys., 18, 11261-11275, https://doi.org/10.5194/acp-18-11261-2018, 2018.

Wu, L., Zhang, X., Sun, J., Wang, Y., Zhong, J., and Meng, Z.: Intensified wintertime secondary inorganic aerosol formation during heavy haze pollution episodes (HPEs) in Beijing, China, J. Environ. Sci.-China, https://doi.org/10.1016/j.jes.2022.01.008, 2022.

Xiao, Y., Hu, M., Li, X., Zong, T., Xu, N., Hu, S., Zeng, L., Chen, S., Song, Y., Guo, S., and Wu, Z.: Aqueous secondary organic aerosol formation attributed to phenols from biomass burning, Sci. Total

Environ., 847, 157582, https://doi.org/10.1016/j.scitotenv.2022.157582, 2022.

Xu, W., Croteau, P., Williams, L., Canagaratna, M., Onasch, T., Cross, E., Zhang, X., Robinson, W., Worsnop, D., and Jayne, J.: Laboratory characterization of an aerosol chemical speciation monitor with PM2.5 measurement capability, Aerosol Sci. Tech., 51, 69-83, 2017.

Xu, W., Han, T., Du, W., Wang, Q., Chen, C., Zhao, J., Zhang, Y., Li, J., Fu, P., Wang, Z., Worsnop, D. R., and Sun, Y.: Effects of Aqueous-Phase and Photochemical Processing on Secondary Organic Aerosol Formation and Evolution in Beijing, China, Environ. Sci. Technol., 51, 762-770, https://doi.org/10.1021/acs.est.6b04498, 2017.

Yan, F., Chen, W., Jia, S., Zhong, B., Yang, L., Mao, J., Chang, M., Shao, M., Yuan, B., Situ, S., Wang, X., Chen, D., and Wang, X.: Stabilization for the secondary species contribution to PM2.5 in the Pearl River Delta (PRD) over the past decade, China: A meta-analysis, Atmos. Environ., 242, 117817, https://doi.org/10.1016/j.atmosenv.2020.117817, 2020.

Yu, L., Smith, J., Laskin, A., Anastasio, C., Laskin, J., and Zhang, Q.: Chemical characterization of SOA formed from aqueous-phase reactions of phenols with the triplet excited state of carbonyl and hydroxyl radical, Atmos. Chem. Phys., 14, 13801-13816, https://doi.org/10.5194/acp-14-13801-2014, 2014.

Zhai, S., Jacob, D. J., Wang, X., Liu, Z., Wen, T., Shah, V., Li, K., Moch, J. M., Bates, K. H., Song, S., Shen, L., Zhang, Y., Luo, G., Yu, F., Sun, Y., Wang, L., Qi, M., Tao, J., Gui, K., Xu, H., Zhang, Q., Zhao, T., Wang, Y., Lee, H. C., Choi, H., and Liao, H.: Control of particulate nitrate air pollution in China, Nat. Geosci., 14, 389-395, https://doi.org/10.1038/s41561-021-00726-z, 2021.

Zhan, B., Zhong, H., Chen, H., Chen, Y., Li, X., Wang, L., Wang, X., Mu, Y., Huang, R., George, C., and Chen, J.: The roles of aqueous-phase chemistry and photochemical oxidation in oxygenated organic aerosols formation, Atmos. Environ., 266, 118738, https://doi.org/10.1016/j.atmosenv.2021.118738, 2021.

Zhang, L., Guo, X., Zhao, T., Gong, S., Xu, X., Li, Y., Luo, L., Gui, K., Wang, H., Zheng, Y., and Yin, X.: A modelling study of the terrain effects on haze pollution in the Sichuan Basin, Atmos. Environ., 196, 77-85, https://doi.org/10.1016/j.atmosenv.2018.10.007, 2019.

Zhang, Q., Jimenez, J. L., Canagaratna, M. R., Ulbrich, I. M., Ng, N. L., Worsnop, D. R., and Sun, Y.: Understanding atmospheric organic aerosols via factor analysis of aerosol mass spectrometry: a review, Anal. Bioanal. Chem., 401, 3045-3067, https://doi.org/10.1007/s00216-011-5355-y, 2011.

Zhang, Q., Worsnop, D. R., Canagaratna, M. R., and Jimenez, J. L.: Hydrocarbon-like and oxygenated organic aerosols in Pittsburgh: insights into sources and processes of organic aerosols, Atmos. Chem. Phys., 5, 3289-3311, https://doi.org/10.5194/acp-5-3289-2005, 2005.

Zhang, Y. W., Zhang, X. Y., Zhang, Y. M., Shen, X. J., Sun, J. Y., Ma, Q. L., Yu, X. M., Zhu, J. L., Zhang, L., and Che, H. C.: Significant concentration changes of chemical components of PM1 in the Yangtze River Delta area of China and the implications for the formation mechanism of heavy haze–fog pollution, Sci. Total Environ., 538, 7-15, https://doi.org/10.1016/j.scitotenv.2015.06.104, 2015.

Zhao, D., Liu, G., Xin, J., Quan, J., Wang, Y., Wang, X., Dai, L., Gao, W., Tang, G., Hu, B., Ma, Y., Wu, X., Wang, L., Liu, Z., and Wu, F.: Haze pollution under a high atmospheric oxidization capacity in summer in Beijing: insights into formation mechanism of atmospheric physicochemical processes, Atmos. Chem. Phys., 20, 4575-4592, https://doi.org/10.5194/acp-20-4575-2020, 2020.

Zhao, J., Qiu, Y., Zhou, W., Xu, W., Wang, J., Zhang, Y., Li, L., Xie, C., Wang, Q., Du, W., Worsnop, D. R., Canagaratna, M. R., Zhou, L., Ge, X., Fu, P., Li, J., Wang, Z., Donahue, N. M., and Sun, Y.: Organic Aerosol Processing During Winter Severe Haze Episodes in Beijing, J. Geophys. Res.-Atmos., 124, 10248-10263, https://doi.org/10.1029/2019JD030832, 2019.

Zhao, R., Mungall, E. L., Lee, A. K. Y., Aljawhary, D., and Abbatt, J. P. D.: Aqueous-phase photooxidation of levoglucosan – a mechanistic study using aerosol time-of-flight chemical ionization mass spectrometry (Aerosol ToF-CIMS), Atmos. Chem. Phys., 14, 9695-9706, https://doi.org/10.5194/acp-14-9695-2014, 2014.

Zheng, G. J., Duan, F. K., Su, H., Ma, Y. L., Cheng, Y., Zheng, B., Zhang, Q., Huang, T., Kimoto, T., Chang, D., Pöschl, U., Cheng, Y. F., and He, K. B.: Exploring the severe winter haze in Beijing: the impact of synoptic weather, regional transport and heterogeneous reactions, Atmos. Chem. Phys., 15, 2969-2983, https://doi.org/10.5194/acp-15-2969-2015, 2015.

Zheng, G., Duan, F., Ma, Y., Zhang, Q., Huang, T., Kimoto, T., Cheng, Y., Su, H., and He, K.: Episode-Based Evolution Pattern Analysis of Haze Pollution: Method Development and Results from Beijing, China, Environ. Sci. Technol., 50, 4632-4641, https://doi.org/10.1021/acs.est.5b05593, 2016.

Zhou, W., Chen, C., Lei, L., Fu, P., and Sun, Y.: Temporal variations and spatial distributions of gaseous and particulate air pollutants and their health risks during 2015–2019 in China, Environ. Pollut., 272, 116031, https://doi.org/10.1016/j.envpol.2020.116031, 2021.